

Journal of Visualized Experiments

Using Retinal Imaging to Study Dementia

--Manuscript Draft--

Manuscript Number:	JoVE56137R2
Full Title:	Using Retinal Imaging to Study Dementia
Article Type:	Invited Methods Article - JoVE Produced Video
Keywords:	Retinal imaging; Dementia; Alzheimer's disease; optical coherence tomography; Fundus photography; Singapore I Vessel Assessment; Retinal microvasculature; Small vessel disease; Retinal Nerve Fibre Layer; Ganglion Cell-Inner Plexiform Layer
Manuscript Classifications:	3.10.228.140.380: Dementia; 3.10.228.140.380.100: Alzheimer Disease; 3.10.574: Neurodegenerative Diseases; 3.11: Eye Diseases; 5.1.158: Diagnosis, Computer-Assisted; 5.1.370: Diagnostic Techniques and Procedures; 5.5: Investigative Techniques; 6.3.87.400: Dementia; 6.3.87.400.100: Alzheimer Disease; 8.1.158.610: Neurosciences
Corresponding Author:	Carol Cheung Chinese University of Hong Kong Hong Kong, Hong Kong HONG KONG
Corresponding Author Secondary Information:	
Corresponding Author E-Mail:	carolcheung@cuhk.edu.hk
Corresponding Author's Institution:	Chinese University of Hong Kong
Corresponding Author's Secondary Institution:	
First Author:	Victor T.T. Chan
First Author Secondary Information:	
Other Authors:	Victor T.T. Chan
	Tiffany H.K. Tso
	Fangyao Tang
	Clement Tham
	Vincent Mok
	Christopher Chen
	Tien Y. Wong
Order of Authors Secondary Information:	
Abstract:	<p>The retina potentially offers a unique "window" to study pathophysiological processes of dementia in the brain, as it is an anatomical and physiological extension of the central nervous system and shares prominent similarities with the brain in terms of vascular and neuronal structure. The vascular and neuronal structure in the retina can now be visualized non-invasively using widely available retinal imaging techniques, including fundus photography and optical coherence tomography (OCT), and quantified using computer-assisted analysis programs. Studying the associations of vascular and neuronal changes in the retina with dementia could improve our understanding of dementia and, potentially, aid the diagnosis and risk assessment. This protocol aims to describe a method of quantifying and analyzing retinal vasculature and neuronal structure using retinal imaging techniques. This protocol also provides examples of retinal changes in subjects with dementia and discusses the technical issues of retinal imaging.</p>

Author Comments:	<p>The co-author "Vincent Mok" has three affiliations in total:</p> <p>(a) Department of Medicine & Therapeutics, The Chinese University of Hong Kong, Hong Kong</p> <p>(b) Therese Pei Fong Chow Research Centre for Prevention of Dementia, The Chinese University of Hong Kong, Hong Kong</p> <p>(c) Gerald Choa Neuroscience Centre, The Chinese University of Hong Kong, Hong Kong</p> <p>Thank you!</p>
Additional Information:	
Question	Response
If this article needs to be "in-press" by a certain date, please indicate the date below and explain in your cover letter.	

TITLE:

Using Retinal Imaging to Study Dementia

AUTHORS & AFFILIATIONS:

Victor T.T. Chan¹, Tiffany H.K. Tso¹, Fangyao Tang¹, Clement Tham¹, Vincent Mok^{2,3,4}, Christopher Chen^{5,6}, Tien Y. Wong^{7,8}, Carol Y. Cheung¹

¹Department of Ophthalmology and Visual Sciences, The Chinese University of Hong Kong, Hong Kong

²Department of Medicine & Therapeutics, The Chinese University of Hong Kong, Hong Kong

³Therese Pei Fong Chow Research Centre for Prevention of Dementia, The Chinese University of Hong Kong, Hong Kong

⁴Gerald Choa Neuroscience Centre, The Chinese University of Hong Kong, Hong Kong

⁵Memory Aging and Cognition Centre, National University Health System, Singapore

⁶Department of Pharmacology, National University of Singapore, Singapore

⁷Singapore Eye Research Institute, Singapore National Eye Centre, Singapore

⁸Duke-NUS Medical School, National University of Singapore, Singapore

E-MAIL ADDRESSES:

Victor T.T. Chan (victorttchan@gmail.com)

Tiffany H.K. Tso (jasminetiffy@gmail.com)

Fangyao Tang (tangfangyao@gmail.com)

Clement Tham (clemtham@cuhk.edu.hk)

Vincent Mok (vctmok@cuhk.edu.hk)

Christopher Chen (cplhchen@yahoo.com.sg)

Tien Y. Wong (wong.tien.yin@singhealth.com.sg)

Carol Y. Cheung (carolcheung@cuhk.edu.hk)

CORRESPONDING AUTHOR:

Carol Y. Cheung (carolcheung@cuhk.edu.hk)

Address: CUHK Eye Centre, Hong Kong Eye Hospital, 147K Argyle Street, Kln, Hong Kong

T: +852 3943 5831 / F: +852 2715 9490

KEYWORDS:

Retinal imaging, Dementia, Alzheimer's Disease, Optical Coherence Tomography, Fundus Photography, Retinal microvasculature, Small vessel disease, Retinal Nerve Fiber Layer, Ganglion Cell-Inner Plexiform Layer

SHORT ABSTRACT:

The retina shares prominent homologies with the brain and thus represents a unique window to study vasculature and neuronal structure in the brain non-invasively. This protocol describes a method to study dementia using retinal imaging techniques. This method can potentially aid in the diagnosis and risk assessment of dementia.

LONG ABSTRACT:

The retina potentially offers a unique “window” to study pathophysiological processes of dementia in the brain, as it is an anatomical and physiological extension of the central nervous system and shares prominent similarities with the brain in terms of vascular and neuronal structure. The vascular and neuronal structure in the retina can now be visualized non-invasively using widely available retinal imaging techniques, including fundus photography and optical coherence tomography (OCT), and quantified using computer-assisted analysis programs. Studying the association between vascular and neuronal changes in the retina and dementia could improve our understanding of dementia and, potentially, aid in diagnosis and risk assessment. This protocol aims to describe a method of quantifying and analyzing retinal vasculature and neuronal structure using retinal imaging techniques. This protocol also provides examples of retinal changes in subjects with dementia and discusses the technical issues of retinal imaging.

INTRODUCTION:

Due to increases in life expectancy, dementia has become a major medical problem, contributing to significant social and economic health burden globally¹⁻⁵. Today, a person in the United States develops Alzheimer’s Disease (AD), the most common form of dementia, every 66 s⁶. It has been estimated that by the year 2050, 115 million people will be affected by AD⁷.

The retina offers a unique “window” to study dementia due to its similar anatomical and physiological properties with the brain. In terms of vasculature, the retinal arterioles and venules, measuring 100 to 300 μm in diameter, share similar features with cerebral small vessels, such as end arterioles without anastomoses, barrier function, and auto-regulation^{8,9}. In terms of the neuronal structure, retinal ganglionic cells (RGCs) also share typical properties with neurons in the central nervous system (CNS)¹⁰. The RGCs are prominently connected with the brain as they form the optic nerve and project visual signals from the retina to the lateral geniculate nuclei and the superior colliculus. The optic nerve, similar to many neuronal fibers in the CNS, is myelinated by oligodendrocytes and is ensheathed in meningeal layers. Notably, an insult to the optic nerve can result in similar responses observed in other CNS axons, such as retrograde and anterograde degeneration of the axon, scar formation, myelin destruction, secondary degeneration, and an abnormal level of neurotrophic factors and neurotransmitters¹¹⁻¹⁴. The association of visual symptoms with AD may also be manifested by the robust connection between the retina and the brain^{15,16}. Given these associations between the retina and the brain, it has been suggested that the retina may reflect the subclinical pathophysiological process of dementia in the brain and thus can be used to study dementia.

The retinal vasculature and retinal neuronal structure can now be visualized and quantified non-invasively using retinal imaging techniques. For instance, retinal fundus photographs can be captured using retinal fundus cameras, and characteristics of the retinal vasculature (*e.g.*, vessel caliber, tortuosity, and fractal dimensions) can then be quantified using computer-assisted analysis programs. In addition, parameters of retinal neuronal structure (such as the thickness of ganglion cell-inner plexiform layer [GC-IPL] and retinal nerve fiber layer [RNFL]) can also be

measured using optic coherence tomography (OCT) and quantified using the built-in analysis program.

In view of the importance of retinal imaging to studying dementia, this protocol aims to describe a method of quantifying and analyzing retinal vasculature and neuronal structure *in vivo* using widely available retinal imaging techniques. This protocol also provides examples of retinal changes in subjects with dementia and discusses technical issues related to retinal imaging.

PROTOCOL:

All methods described here have been approved by a local clinical research ethics committee in Hong Kong.

Note: For simplicity, the equipment listed in the **Table of Materials** is used to illustrate the procedures of retinal imaging and subsequent analysis. Quantification of retinal vasculature is performed with the Singapore I Vessel Assessment program (version 4.0)¹⁷ (National University of Singapore, Singapore). This protocol can be performed using a different set of equipment and although the operation of different equipment may vary, the underlying principles remain similar.

1. Prepare Subjects for Retinal Imaging

1.1 Dilate the pupil of the subject using mydriatic agents. Wait for at least 15 min to establish sufficient pupil dilation.

2. Acquire Fundus Photographs of Retinal Vasculature

[Place Figure 1 Here]

2.1. Capture an ocular fundus photograph using the fundus camera.

2.1.1 Start the fundus camera and launch the image capturing program on the computer. Rest the chin of the subject properly on the chinrest with the forehead against the head strap. Move the control lever to align the light beam properly to the subject's pupil. Ensure the distance between the subject's eyes and the main body is no longer than the proper working distance.

2.1.2 Align the illumination points until they appear smallest on both sides in the viewfinder. Move the external fixation target to guide the subject's eyes until the optic disc is at the center of the viewfinder and the regions of interest (ROI) are well within the limits of the image. Adjust the focusing knob to focus on the retina.

2.1.3 Have the subject firmly look at the external fixation target and ensure the subject's eyes are not filled with tears.

2.1.4 Depress the shutter-release button to capture an image (**Figure 1A**).

2.1.5 Check the quality of the fundus photograph captured, using **Figure 2A** as a standard. Discard the image and repeat the image acquisition process (*i.e.*, **Step 2.1.1 to 2.1.4**) if the pupil is poorly dilated (**Figure 2B**), the optic disc is not at the center of the photograph (**Figure 2C**), or the focus is not accurate (**Figure 2D**).

[Place Figure 2 Here]

2.1.6 Save all images in TIFF format with gradable resolution (*i.e.*, approximately 3,000 pixels x 2,000 pixels, at more than 150 dpi).

Note: The protocol can be paused here.

2.2. Open the images in the computer-assisted analysis program for automatic tracing.

Note: The SIVA program is used for illustration purposes only and can be substituted by other available measurement programs.

2.2.1 Select a random sample of 10% of the images and measure the height of the optic discs in these images (see **Figure 3**). Calculate the image conversion factor (ICF) using the formula:
$$\text{ICF} = 1800 \mu\text{m} / (\text{Average pixel height of optic discs of the images sampled}).$$

2.2.2 Upload the captured fundus photographs to the cloud-based server and enter relevant study details, including the image conversion factor (ICF) (**Figure 1B**).

Note: The protocol can be paused here. Other computer-assisted analysis programs may use other non-cloud-based methods to organize the images.

[Place Figure 3 Here]

2.2.3 Open the images with the computer-assisted analysis program (**Figure 1C**). Observe that the program automatically detects the optic disc, places a measurement grid, and traces the vessel paths (**Figure 1D to 1F**).

2.3. Adjust the auto-tracing results of the retinal vasculature. Begin the inspection from the 12 o'clock position in a clockwise manner to ensure that all vessel tracings on the image are verified.

2.3.1. Check that the optic disc is accurately detected and the measurement grid is correctly placed. Adjust the measurement grid manually following steps 2.3.1.1 to 2.3.1.4, if the innermost circle does not accurately outline the optic disc rim (**Figure 4A**).

2.3.1.1 Click the "OD Center" button on the left function panel; the mouse cursor will be replaced by a green circle.

2.3.1.2 Move the green circle to the center of the optic disc (OD), and left-click to fix the circle.

2.3.1.3 Click the “Find OD” button to prompt the software to detect the OD rim and place a new measurement grid based on the new position of the OD center.

2.3.1.4 Click the “Process” button to initiate the auto-tracing process of the vessels.

2.3.2 Left click to select the vessels with incorrect vessel labels (arterioles versus venules) and click the “Vessel (T)ype” button to change the vessel type.

Note: Arterioles can be distinguished from venules based on their physiological differences. For example, venules are generally darker in color and wider than arterioles. Vessels with the same vessel type do not cross each other. Arterioles are labelled in red and venules are labelled in blue.

2.3.3 Extend the incomplete vessel tracings following steps 2.3.3.1 to 2.3.3.2 (**Figure 4B**).

2.3.3.1 Use the cursor to click at the distal end of the incomplete vessel tracing. Left click at points along the vessel to extend the vessel tracing.

2.3.3.2 Press “Esc” to end the tracing process when the end of the vessel is reached. Stop the tracing at the outermost white circle if the distal part of the vessel falls outside the measurement grid (see **Figure 4B**).

2.3.4 Adjust the vessel tracings if the vessel path is inaccurately traced at the crossover site (**Figure 4C**).

2.3.4.1 Click the “Select” button and then click at the point on the vessel tracing to be disconnected. Click the “Brea(k) Seg” button to disconnect the vessel tracing at the point selected. Select the disconnected segment and click the “(Del) Seg” button to delete it.

2.3.4.2 Repeat steps 2.3.3.1 and 2.3.3.2 to re-construct the remaining segment.

2.4 Lay vessel covers on all vessel segments and adjust the covers manually.

2.4.1 Click the “Find Covers” button to lay vessel covers on all vessel segments automatically.

Note: Vessel covers are measurement lines that estimate the approximate width of the internal lumens of the vessels.

2.4.2 Check if all vessel covers are correctly placed for all vessel segments. Left-click and drag the cursor over vessel covers to deactivate them if the vessel covers are not laid perpendicular to the vessel walls (**Figure 5A**), the vessel is obscured under another vessel (**Figure 5B**), or the vessel covers overestimate or underestimate the width of the internal lumen (**Figure 5C**).

2.5. Close the grading windows and click “send” in the pop-up dialog to upload the graded image to the cloud-based server for automatic measurement.

[Place Figure 4 Here]

[Place Figure 5 Here]

3. Measure the Retinal Vascular Parameters Using a Computer-Assisted Analysis Program.

Note: Steps 3.1 to 3.7 can be completed automatically by a computer-assisted analysis program.

3.1 Open the fundus photograph to be measured.

3.2 Place four concentric circles as measurement grids using the center of optic disc as a reference (**Figure 6A**). Label the area 0.5-1.0 disc diameters away from the disc margin as zone B, and the area 0.5-2.0 disc diameters away from the disc margin as zone C¹⁸ (**Figure 6A**), according to the modified protocol of Atherosclerosis Risk in Communities (ARIC) study¹⁹.

3.3 Measure retinal vascular caliber from both zone B and zone C, using a method modified from the ARIC study¹⁹ (**Figure 6B**). This has been widely adopted in many large population studies^{20–26}.

3.3.1 Measure the lengths of vessel covers in the six largest arterioles and the six largest venules to estimate retinal vessel calibers.

3.3.2 Summarize the retinal arteriolar and venular calibers as central retinal artery equivalent (CRAE) and central retinal vein equivalent (CRVE) respectively¹⁷, using the revised Knudtson–Parr-Hubbard formula^{18,19}.

[Place Figure 6 Here]

3.4 Identify all vessels in zone C with a width $>40\ \mu\text{m}$. Calculate the retinal arteriolar and venular tortuosity from the integral of the total squared curvature along the vessel paths and normalize the value with the total arc length, bowing, and points of inflection^{27,28}.

3.5 Compute the total, arteriolar, and venular fractal dimensions from zone C, using the established “box-counting method”^{29–31}.

3.5.1 Divide the retinal image into a series of equally sized square boxes.

3.5.2 Count the number of boxes containing a section of the skeletonized line tracing.

3.5.3 Repeat the process with a series of different sized boxes.

3.5.4 Plot the logarithm of the number of boxes containing the line tracing against the logarithm of the size of the boxes, and calculate the slope of the resulting line; this is the fractal dimension.

3.6 Identify vessels with first bifurcation in zone C and calculate the angles (θ) subtended between the first two daughter vessels³² (**Figure 6C**). Compute the mean value to obtain the average branching angle.

3.7 Calculate the branching coefficient from zone C using the formula: $(d_1^2 + d_2^2)/d_0^2$, where d_0 is the mean trunk caliber, and d_1 and d_2 are the mean branch calibers (**Figure 6C**).

4. Assess the Thickness of GC-IPL and RNFL

[Place Figure 7 Here]

4.1. Perform image acquisition using optical coherence tomography (OCT).

4.1.1 Open the OCT program and select the “Macular Cube” scanning protocol to start a new macular scan (**Figure 7A**).

4.1.2 Locate the pupil in the iris viewport by adjusting the chinrest. Lower the illumination if the pupil size is too small.

4.1.3 Click the “Auto Focus” button and then the “Optimize” button to improve the image quality.

4.1.4 Instruct the subject to blink a few times immediately before starting the scan.

4.1.5 Click the “Capture” button to start the scan when the border surrounding the button becomes green. Instruct the subject to focus on the visual fixation target to avoid motion artifacts.

4.1.6 Perform an optic nerve head scan with the “Optic Disc Cube” scanning protocol using steps 4.1.2 to 4.1.5 (**Figure 7B**).

4.1.7 Review the quality of the captured scan using **Figure 7C** and **7D** as a standard. Discard the image and retake the scan if the signal strength is smaller than 6 (**Figure 8A**), or motion artefacts are detected (indicated by discontinuity of blood vessels) (**Figure 8B**).

4.1.8 Save the scanning results.

[Place Figure 8 Here]

4.2. Generate the analysis printout of the macular GC-IPL thickness.

4.2.1 Select the “Macular Cube” scan records of both eyes in the analysis interface.

4.2.2 Click the “Ganglion Cell OU Analysis” to initiate the automatic analysis algorithm to assess the GC-IPL thickness of the captured image (**Figure 7E**).

Note: Steps 4.2.2.1 to 4.2.2.4 can be automatically completed by the analysis algorithm.

4.2.2.1 Generate a 14.13 mm² fovea-centered elliptical annulus that has horizontal inner and outer radiuses of 0.6 mm and 2.4 mm, respectively, and vertical inner and outer radiuses of 0.5 mm and 2.0 mm, respectively.

Note: The size and shape of the elliptical annulus conform closely to the macular anatomy and thus correspond to the area where the RGCs are thickest in normal eyes^{33,34}. The area within the inner ring of the annulus is not measured, since the macular GC-IPL in this area is very thin and difficult to detect accurately.

4.2.2.2 Segment the outer boundary of the RNFL and the outer boundary of the inner plexiform layer (IPL) to locate the GC-IPL (**Figure 9**).

4.2.2.3 Measure the average, minimum, and six sectorial (superotemporal, superior, superonasal, inferonasal, inferior, inferotemporal) thickness of macular GC-IPL within the fovea-centered elliptical annulus.

4.2.2.4 Report the measurement results on an analysis printout.

4.2.3 Save the analysis printout in the .pdf format.

[Place Figure 9 Here]

4.3. Generate the analysis printout of the RNFL thickness (**Figure 7F**).

4.3.1 Select the “Optic Disc Cube” scan records of both eyes in the analysis interface.

4.3.2 Click the “ONH and RNFL OU Analysis” to initiate the automatic analysis algorithm to assess the RNFL thickness of the captured image.

Note: Steps 4.3.2.1 to 4.3.2.6 can be automatically completed by the analysis algorithm.

4.3.2.1 Measure the RNFL thickness at each scan point and generate an RNFL thickness map.

4.3.2.2 Identify the optic disc by detecting a dark spot near the center of the scan that has a size and shape consistent with the range of an optic disc.

4.3.2.3 Position a calculation circle of 3.46 mm in diameter around the optic disc on the RNFL

thickness map.

4.3.2.4 Measure and calculate the global, four-quadrants (temporal, superior, nasal and inferior), and twelve-clock-hour parapapillary RNFL thickness, using the calculation circle as the region of interest (ROI).

4.3.2.5 Compare the measured RNFL thickness to the device's internal normative age-matched database and generate a deviation map and a significance map.

4.3.2.6 Report the measurement results on an analysis printout.

4.3.3 Save the analysis printout in the .pdf format.

REPRESENTATIVE RESULTS:

[Place Figure 10 Here]

Interpretation of the Retinal Vascular Parameters: Through the protocol described, several quantitative retinal vascular parameters can be measured from the fundus photographs. These parameters indicate the status of the retinal vasculature, which may in turn reflect similar changes in the cerebral vasculature. **Figure 10** shows the fundus photographs obtained from an AD subject and a healthy subject and their retinal vascular parameters are reported in **Table 1**. These two fundus photographs were analyzed using the method described in this protocol and are used as an example to demonstrate the interpretation of the retinal vascular parameters.

[Place Table 1 Here]

Retinal Vessel Caliber: The fundus photograph of the AD subject shown in **Figure 10** showed a decrease in CRAE and CRVE of Zone C (138.47 μm and 206.61 μm , respectively), when compared to the healthy subject (165.82 μm and 232.22 μm , respectively). The CRAE and CRVE summarize the retinal vessel calibers, which approximates the average width of the internal lumen in retinal arterioles and venules, respectively. Reduction in CRAE or CRVE thus indicates generalized retinal vessel narrowing, and may suggest subtle microvascular dysfunction³⁵.

Retinal Vascular Network Parameters: Firstly, the retinal arteriolar and venular tortuosity of the AD subject (0.613×10^{-4} and 1.41×10^{-4} , respectively) were higher than that of the normal subject (0.476×10^{-4} and 0.501×10^{-4} , respectively). The higher vascular tortuosity value indicates that the retinal vessels are generally straighter in the AD subject.

Secondly, the AD subject also had reduced retinal fractal dimension (total fractal dimension, 1.472; arteriolar fractal dimension, 1.246; venular fractal dimension, 1.253) when compared to the healthy subject (total fractal dimension, 1.517; arteriolar fractal dimension, 1.316; venular fractal dimension, 1.273). Since fractal dimension represents a “global” measure that summarizes

the branching complexity of the retinal vascular network³⁰, a smaller value in the AD subject indicates a less complex branching pattern.

Thirdly, most retinal bifurcation parameters of the AD subject were deviated from the optimal value. Specifically, the arteriolar and venular branching angle of the AD subject (67.17° and 60.109° , respectively) were further away from optimal values, which are approximately 75° , when compared with the normal subject (81.16° and 73.19° , respectively)³⁶. Furthermore, the arteriolar branching coefficient of the AD subject (2.432) was also severely deviated from the optimal value, which is approximately 1.26³⁶. This represents an increase in the total cross-sectional area across the bifurcations³⁷.

Interpretation of Retinal Neuronal Parameters: Through the protocol described, one should obtain two analysis printouts showing the parameters of RNFL thickness and the GC-IPL thickness (illustrated in **Figure 11A and 11B**, respectively). While the RNFL measurements reflect the health of the unmyelinated axons of RGCs, the GC-IPL measurements indicate the health of the cell bodies and dendrites of RGCs. Since the size of RGC cell body is 10-20 times the diameter of their axons, GC-IPL thickness has been shown to be more strongly related to cognitive impairment³⁸. In both reports, three maps were shown to aid the subsequent analysis, namely (a) thickness maps, (b) deviation maps, and (c) significance maps.

In the thickness map, warmer colors represent higher thickness values and cooler colors represent lower thickness values; in other words, the denser the orange/yellow ring, the thicker the retinal layer. In the deviation maps of both reports, a super-pixel is shown in red or yellow if the thickness value falls outside the 99% or within 95%–99% centile range, respectively. In addition, the analysis algorithm also compares the measurement results with the normative database and reports the findings as a significance map. The significance map of the GC-IPL thickness is reported in the form of six sectors, while that of the RNFL thickness is reported in a form of four quadrants and 12 clock-hours. All types of significance maps are color-coded to match the thickness, with values within the normal range in green ($p=5\%–95\%$), borderline values in yellow ($1\%<p<5\%$), and values outside the normal range in red ($p<1\%$). Numeric values inside or near sectors represent average thickness in the corresponding sectors.

Figure 11A and Figure 11B are the analysis printouts obtained from an AD subject. The fading of warm colors and the appearance of light blue areas in the thickness maps indicates the thinning of the GC-IPL and the RNFL in the AD subject. While the former change suggests RGC loss, the latter change suggests a loss of RGC axons. In addition, several sectors of the significance maps are labelled in red or yellow, suggesting that the RNFL and GC-IPL thickness of these sectors are reduced in the AD subject. The exact location of thickness reduction is also visualized by the red or yellow super-pixels in the deviation maps.

[Place Figure 11 Here]

Unanalyzable or Ungradable Retinal Images: Unanalyzable retinal images may be obtained for several reasons. For instance, GC-IPL or RNFL segmentation failure may occur due to retinal

pathologies, including age-related macular degeneration, diabetic retinopathy, and epiretinal membrane. **Figure 12A** demonstrates an example of segmentation failure due to diabetic macular edema. OCT studies have also shown that OCT scan quality and thickness measures can be affected by dry eyes³⁹, cataracts^{40–43}, floaters and other vitreous opacities^{44,45}. In addition, the retinal vasculature analysis may also be hindered by media opacity (such as a cataract), which affects the visibility of the retinal vasculature (**Figure 12B**).

[Place Figure 12 Here]

FIGURES and TABLE LEGENDS

Figure 1. Schematic diagram showing the procedures of retinal vasculature measurement.

(A) Ocular fundus photography is used to obtain an optic-disc-centered fundus photography. **Figure 1A** is identical to **Figure 2A**, both of which represent an optimal quality of fundus photograph. (B) Upload the captured images to the cloud-based server and enter relevant study details, including the image conversion factor (ICF). (C) Download and open the fundus photographs from the cloud-based server in the program. (D, E, F) The program automatically detects the optic disc, places a measurement grid, and traces the vessel paths. (G) The graders are required to check the accuracy of the auto-tracings and, if necessary, perform manual adjustments. (H) After confirming the accuracy of all tracings, a spectrum of retinal vascular parameters, including vessel calibers, tortuosity, fractal dimension and bifurcation, will be measured automatically. Step (D) to Step (F) can be done automatically by the computer-assisted analysis program.

Figure 2. Optimal and suboptimal fundus photographs. The image quality of fundus photographs directly affects the measurement and analysis of the retinal microvasculature. Hence, the quality of fundus photographs must be checked immediately after image acquisition. The image should be discarded if one of these artefacts is observed. These images were captured using a 50-degree fundus camera.

Figure 3. A schematic diagram illustrating the calculation of the image conversion factor (ICF).

To calculate the ICF, randomly select a 10% sample of images from the total number of images expected from the study (Step 1). Then, measure optic disc height in pixels from sample images (Step 2). Calculate the ICF using the formula: $ICF = 1800 \mu m / (\text{Average pixel height of optic discs from sample images})$, where $1800 \mu m$ is the estimated height of a normal optic disc (Step 3). As magnification effect and image resolution differ from camera to camera, it is necessary to calculate an accurate ICF for each camera used for every study.

Figure 4. Common errors of the auto-tracing. The auto-tracing of the program is not completely accurate and manual adjustments are required to ensure the accuracy of the measurement. This figure shows common errors of the auto-tracing and demonstrates optimal results after manual adjustments. (A) Incorrect detection of the optic disc could lead to misplacement of the measurement grid and affect the subsequent measurements. Ideally, the innermost circle should outline the optic disc rim. (B) Incomplete vessel tracing could lead to the incorrect measurement of fractal dimension, tortuosity, etc. The vessel path should be traced until the end of the vessel.

If the distal part of the vessel falls outside the measurement grid, the tracing can be stopped at the outermost white circle. (C) Vessel tracings at the crossover sites are subject to a higher tendency for error and thus require special attention.

Figure 5. Incorrect vessel covers. This figure shows examples of incorrect vessel covers that should be deactivated and excluded from the measurement. (A) Vessel covers should be deactivated if they are irregular and not perpendicular to vessel walls. (B) Vessel covers should be deactivated if the vessel being traced is obscured under another vessel (C) Vessel covers should be deactivated if they cannot represent the approximate width of the vessel.

Figure 6. Quantification of retinal vasculature. (A) Zone B (defined as 0.5-1.0 disc diameters away from the disc margin) is used to measure vessel calibers of zone B according to the Atherosclerosis Risk in Communities Study. Zone C (defined as 0.5-2.0 disc diameters away from the disc margin) is used to measure vessel calibers of zone C and a spectrum of retinal vascular network parameters (such as tortuosity, fractal dimension, and bifurcation). (B) Vessel covers are measurement lines used to estimate the retinal vascular calibers (or retinal vessel diameters). Incorrect vessel covers can be manually excluded from the measurement. (C) At each bifurcation, the program automatically detects the branching angles (θ) of all vessels that have their first bifurcation within zone C. In addition, the branching coefficient is also calculated using the formula: Branching coefficient = $(d_1^2 + d_2^2)/d_0^2$, where d_0 is the trunk caliber, and d_1 and d_2 are the branch calibers.

Figure 7. Image acquisition and optimal results of retinal neuronal structure analysis. Optical coherence tomography (OCT) is used to measure the thickness of the ganglion cell-inner plexiform layer (GC-IPL) and retinal nerve fiber layer (RNFL). (A, B) The GC-IPL and RNFL can be imaged using the built-in “macular cube” and “optic disc cube” scanning protocols respectively. (C, D) It is critical to check the image quality immediately after image acquisition. Discard the image and retake the scan if the signal strength is smaller than 6, or motion artefacts are detected. (E, F) After finishing the image acquisition, the built-in algorithm can automatically analyze the image and generate a report for interpretation.

Figure 8. Sub-optimal results of optical coherence tomography. Common sub-optimal results of the optical coherence tomography (OCT) include (A) poor signal strength (strength value <6), and (B) motion artefacts. The quality of OCT images should be checked immediately after image acquisition, and the scan protocol should be repeated if these artefacts are observed.

Figure 9. Retinal layers used for the assessment of the retinal neuronal structure. The ganglion cell analysis (GCA) algorithm detects the outer boundary of the retinal nerve fiber layer (RNFL) and the inner plexiform layer (IPL) to yield the combined thickness of the GCL and the IPL. The thicknesses of the GCL and the IPL are measured together, as the boundary between the GCL layer and the IPL is anatomically indistinct, but the combined thickness is indicative of the health of RGCs. The measurement of the RNFL is done using the HD-OCT optic nerve head (ONH) algorithm, while the measurement of the GC-IPL is done using the HD-OCT ganglion cell analysis (GCA) algorithm.

Figure 10. An example to show the differences in retinal vasculature between a normal subject and an AD subject. (A) Fundus photographs of a healthy subject showing wider vessel caliber (CRAE of Zone B, 156.45 μm ; CRVE of Zone B, 207.54 μm ; CRAE of Zone C, 165.82 μm ; CRVE of Zone C, 232.22 μm), higher retinal vascular fractal dimension (total fractal dimension, 1.517; arteriolar fractal dimension, 1.316; venular fractal dimension, 1.273) and smaller retinal vascular tortuosity (arteriolar tortuosity [10^4], 0.476; venular tortuosity [10^4], 0.501). (B) Fundus photographs of an AD subject showing narrower vessel caliber (CRAE of Zone B, 116.38 μm ; CRVE of Zone B, 186.93 μm ; CRAE of Zone C, 138.47 μm ; CRVE of Zone C, 206.61 μm), smaller retinal vascular fractal dimension (total fractal dimension, 1.472; arteriolar fractal dimension, 1.246; venular fractal dimension, 1.253) and higher retinal vascular tortuosity (arteriolar tortuosity [10^4], 0.613; venular tortuosity [10^4], 1.41). These images were captured using 50-degree fundus camera and were analyzed using the method described in the protocol.

Figure 11. Analysis printout of the retinal neuronal structure from a subject with AD. The analysis printouts of both GC-IPL and RNFL thickness include three types of thickness map, namely the thickness map, the deviation map, and the significance map. (A) The red and yellow super-pixels in the right deviation map (red arrows) indicate the RNFL thickness of these parts of the retina fell outside the 99% or within 95%–99% percentile range, respectively. Consistently, the decreased RNFL thickness of these regions is also indicated by the red and yellow sectors in the two significance maps, namely “RNFL quadrants” and “RNFL clock hours”. While the red sectors indicate the RNFL thickness fell outside the normal range ($p < 1\%$), the yellow sector indicates borderline values ($1\% < p < 5\%$). All together, these maps suggest that the RNFL thickness was reduced in the AD subject. (B) The interpretation of the GC-IPL thickness is similar to that of the RNFL thickness. In the AD subject, the thickness map shows light blue areas (red arrows), which visualize the thinning of the GC-IPL. In line with this finding, the red and yellow super-pixels in the deviation maps (red arrows) also indicate the thickness of these regions fell outside the 99% or within 95%–99% percentile range, respectively. Reduction of GC-IPL thickness in these regions is also illustrated by the red sectors in the significance map.

Figure 12. Unanalyzable or ungradable images. Most suboptimal results could be corrected using the methods described in the protocol. However, several types of retinal images are unanalyzable and should be discarded. (A) In the OCT, segmentation failure may occur due to retinal pathologies, including age-related macular degeneration, diabetic retinopathy, and epiretinal membrane. This figure demonstrates a segmentation failure due to diabetic macular edema. (B) The visibility of the retinal microvasculature is reduced by media opacity, such as opacity due to a cataract. This figure demonstrates that severe media opacity can render the image unanalyzable.

Figure 13. Retinal imaging is a potentially valuable tool to study vascular and neuronal changes associated with dementia. It has been proposed that dementia is associated with neuronal injury and small vessel disease in the brain. Given the retina, an extension of the central nervous system, shares prominent similarities with the brain, these pathophysiological changes may be reflected in the retina as retinal neuronal and vascular damage. With the methods described in

this protocol, the retinal neuronal changes can be quantified as the thickness of RNFL and GC-IPL using optical coherence tomography (OCT), while the retinal vascular changes can be quantified as vessel calibers and vascular network parameters using fundus photography and computer-assisted analysis program. Studying the associations between the retinal changes and dementia may provide new insights into the pathophysiology of dementia and, potentially, aid in diagnosis and risk assessment.

Table 1. Retinal Vascular Parameters of an AD subject and a normal subject. The fundus photographs of these two subjects are shown in **Figure 10**. The AD subject showed reductions in CRAE and CRVE, fractal dimension, and an increase in tortuosity. In addition, the branching angles and coefficients of the AD subject also deviated from optimal values.

Table 2. Interpretations of major retinal vascular parameters. Vessel calibers and retinal vascular network parameters are two main categories of parameters reported by the computer-assisted analysis program. CRAE and CRVE document generalized retinal vessel narrowing or widening, reflecting subtle retinal microvascular dysfunction. Retinal vascular network parameters capture the “optimality” and “efficiency” of blood distribution in the retinal network, which in turn reflect the integrity of the cerebral microcirculation.

DISCUSSION:

This protocol describes retinal imaging methods to study retinal neuronal and microvascular structures *in vivo*. As retinal changes reflect different aspects of the vasculature and neuronal structure in the brain, this method can be used to study dementia and, potentially, aid in diagnosis and risk assessment.

In the illustrated example shown in **Figure 10** and **Table 1**, the AD subject showed decreased vessel caliber. Consistently, it has been reported that increased CRVE is associated with incident dementia⁴⁶ and vascular dementia⁴⁶, and decreased CRVE and CRAE are associated with Alzheimer’s Disease^{47,48}.

Furthermore, the AD subject also showed decreased fractal dimension, increased vascular tortuosity, and a suboptimal branching coefficient and branching angle when compared to the normal subject. These changes indicate the alterations in global geometrical patterns of the retinal vascular network^{49–56}. Since the branching pattern of the vascular network, according to Murray’s principle, is structurally developed to minimize the energy required to maintain blood flow⁵⁷, these parameters capture the “optimality” and “efficiency” of blood distribution in the retinal vascular network, which may in turn reflect the integrity of the cerebral microcirculation⁵⁸. It has been reported that reduced retinal fractal dimension is associated with dementia^{47,48,59} and cognitive function⁶⁰, because retinal hypoxia resulted from retinal vessel rarefaction and collapse may reduce the complexity of the retinal vascular network⁶¹. Increased venular and arteriolar tortuosity are also shown to be associated with AD⁶². Regarding the retinal bifurcation parameters, sub-optimality of the branching angle indicates that the retinal vascular network in the AD subject has decreased efficiency of tissue perfusion and increased energy loss³⁷. Alteration in branching angle may also indicate changes in blood flow^{63,64}, endothelial

dysfunction^{65,66}, and attenuation of oxygen saturation⁶⁷. In addition, deviation from the optimal value of the branching coefficient may also increase energy cost, reducing the efficiency of circulation, and metabolic transport³⁷. The reported associations of major retinal parameters with AD are summarized in **Table 2** and have also been discussed in details previously^{8,58,68,69}.

As illustrated by **Figure 11**, the AD subject also showed decreased thickness of RNFL and GC-IPL. Although the thickness of the GCL and the IPL can only be reported together owing to their ambiguous anatomical boundaries, the combined thickness is indicative of the health of RGCs³⁸. It is increasingly evident that thinning of GC-IPL³⁸ and/ or RNFL^{70–78} is associated with AD. Recently, a large-scale population study also reported that thinner macular RNFL is associated with poorer cognitive function, such as poorer prospective memory and poorer performance of numeric and verbal reasoning⁷⁹. In addition, retinal RGC axonal loss, as indicated by thinning of RNFL, is also reported in non-AD dementias^{80–82}.

Critical Steps of Retinal Imaging: To achieve optimal results, several steps in the protocol require special attention. Regarding the procedure of image acquisition, it is important to master the imaging procedure of OCT and ocular fundus photography, since a prolonged imaging time may induce eye fatigue and thus increase the likelihood of motion artefacts. In addition, the contrast and saturation of the images should be standardized during image acquisition to avoid coarse adjustment in the later steps of image processing. The contrast and the saturation can be varied with different study cohorts and camera types.

Regarding the measurement of retinal vasculature, it is important to calculate the ICF for every camera used in the study to adjust for the magnification effect and the difference in image resolution. Adjustment by ICF is important for the accurate measurement of dimensional parameters, including retinal vessel calibers. In addition, when grading the fundus photographs with the program, graders should be masked to the participant's characteristics as the program involves a certain amount of manual correction. Also, the graders should receive proper training and their reliability of measurement should be evaluated first, before grading the images.

It is also important to report retinal vessel caliber in both zone B and zone C. It is believed that the vessel caliber of zone C is more sensitive and more precise with smaller standard error¹⁷, possibly due to inclusion of more peripheral small vessels in the retina, which are anatomically and physiologically similar to the small vessels in the brain. Hence, the caliber of zone C is used in this protocol to study dementia. However, the caliber of zone B should also be reported as the caliber measurement within zone B has been widely used in numerous epidemiological studies.

It should be emphasized that the equipment and the measurement program used in this protocol are for illustration purposes only and similar results can be obtained using other retinal imaging techniques. However, in most cases the numerical parameters reported by different measurement systems should not be interpreted interchangeably⁸³. Yip *et al.* have developed an algorithm for conversion between three commonly used retinal vessel calibers measurement software, which may be useful to compare results from different studies⁸³.

Significance of Retinal Imaging: Magnetic Resonance Imaging (MRI) and Positron Emission Tomography (PET) imaging are two common *in vivo* imaging methods to study the CNS. However, the application of MRI is limited by its spatial resolution to detect subtle degenerative changes of less than 500 μm . The use of PET imaging is also limited by its high cost and the availability of PET facilities. In addition, although cerebral small vessel disease has been linked to dementia^{84–90}, the limitations of current neuroimaging technologies hinder the direct assessment of the changes in the cerebral small vessels, such as cerebral arteriolar narrowing, changes in vascular tortuosity, and capillary micro-aneurysm. In contrast, retinal imaging demonstrates several features that make it a valuable tool to study dementia.

Firstly, the retina, when compared with other parts of the CNS, is highly accessible for non-invasive imaging in live individuals. As the pupil allows bidirectional passage for the illuminating and imaging light rays, the retina can be imaged directly and rapidly using a fundus camera, which is a classic retinal imaging technique based on the principle of monocular indirect ophthalmoscopy. Fundus photography has demonstrated high sensitivity, specificity, and inter-examination and intra-examination agreement⁹¹. Furthermore, *in vivo* cross-sectional retinal images can now be captured by OCT with high resolution, based on the principle of low-coherence interferometry^{92–96}. After image acquisition, a three-dimensional retinal image can also be constructed by combining cross sections. As a result, retinal imaging allows longitudinal *in vivo* monitoring in all age groups to observe dementia-related changes.

Secondly, the retinal neuronal structure is organized as distinguishable layers and each layer represents different elements of the neuronal architecture. For instance, the GC-IPL represents the retinal ganglionic cells and their dendrites, while the RNFL represents the axons of the retinal ganglionic cells. Notably, accurate demarcation of retinal neuronal layers, such as GC-IPL and RNFL, can now be achieved with advanced segmentation algorithms^{33,97}, and damage that manifests as a distortion of the normal architecture can be easily detectable. Since the retinal neurons share prominent similarities with the CNS neurons, dementia-related changes in the retinal neuronal structure can be used to study the pathological processes of dementia and might be used as prognostic factors for dementia.

Thirdly, objective, semi-automated, and standardized assessment of retinal images is now possible using computer-assisted analysis programs. As illustrated by this protocol, the computer-assisted analysis programs can automatically trace the retinal vasculature captured by the fundus photograph and, based on the tracing results, measure a spectrum of retinal vascular parameters, such as vessel calibers, tortuosity, fractal dimensions, and branching angle. During the measurement process, the graders are only required to verify the results of auto-tracing and, if necessary, adjust incorrect vessel tracings manually. Previous studies have reported that intragrader and intergrader reliability were moderate to high⁴⁹. Similarly, the OCT built-in analysis program can also automatically measure parameters of retinal neuronal structure and compare the results with the normative database, which is not race specific and consists of RNFL measurements of 328 healthy individuals from 5 different ethnic groups⁹⁸. This feature of retinal imaging helps to improve measurement efficiency and consistency by reducing the amount of work required from each grader.

Lastly, retinal imaging technologies can now image the retina at resolutions of several microns, which is at least an order of magnitude than can be achieved with conventional brain imaging techniques. For instance, the spectral domain-OCT can now image the retina in three-dimensional volume at a high scan speed, high axial resolution and a high degree of reproducibility^{99–105}. This allows direct visualization and quantification of subtle changes in the retina.

Taken together, retinal imaging can collect unique information on the cerebral vasculature and neuronal structure that is distinct from current brain imaging techniques, suggesting that retinal imaging may provide a complementary approach to study the pathophysiology of dementia^{9,35,58,68,106–108}.

Limitations of the Method: Retinal imaging is an increasingly popular method to visualize and quantify the microvasculature and neuronal structure in the retina^{8,109}. However, users of this protocol should be aware of its potential limitations for critical interpretation of the results.

First, the quality of ocular fundus photographs and OCT images are affected by a range of ocular factors. For instance, variations in refractive error and axial length may affect the magnification and apparent dimensions of retinal vascular caliber and structures¹¹⁰. Differences in retinal pigmentation, presence of media opacities, photographic technique, camera type (*e.g.*, mydriatic, non-mydriatic, hand-held), and image quality (*e.g.*, brightness, focus, and contrast) may also introduce additional sources of variation and affect measurements^{111–116}. In addition, motion artefacts may be common in an old subject if the image acquisition process is prolonged.

Second, the retinal vascular and neuronal architecture can be affected by many systemic and local pathological processes, and thus some retinal manifestations are not specific to a particular disease. For instance, retinal arteriolar narrowing has been correlated to systemic peripheral vasoconstriction and hypertension, while retinal venular widening has been correlated to endothelial dysfunction, inflammation, and microvascular hypoxia¹¹⁷, and diseases such as cardiovascular disease¹¹⁸ and diabetic retinopathy¹¹⁹. RNFL thinning is also observed in other neurodegenerative diseases, including glaucoma, Parkinson's Disease, and multiple sclerosis¹⁰. It is also noteworthy that age-related reduction in RGCs and RGC axons may occur in the normal retina^{99,120}. These factors limit the potential of retinal imaging as a screening tool.

Third, the associations between retinal changes and dementia remain inconclusive. For instance, the associations of smaller vessel calibers with AD were not replicated by Williams *et al.*⁵⁹, and the association of narrower arteriolar caliber with AD found by the Singapore Epidemiology of Eye Disease program study was also lost after adjusting for confounding cardiovascular factors⁴⁸. Furthermore, increased venular and arteriolar tortuosity in AD has also not been consistently observed^{47,59}. It is also noted that in a large-scale study, the association of arteriolar fractal dimension with dementia was lost in the fully adjusted model⁵⁹.

Fourth, the computer-assisted analysis programs are only semi-automated and require manual adjustment by trained graders^{49,121}. Manual input, even following a standardized protocol, may introduce additional variability in the retinal measurements.

Future applications of the method: In terms of scientific research, given the accessibility of the retina and its similarities with the brain, the retina appears to offer a promising means of studying AD-related changes in the cerebral microvasculature and neuronal structure. Since dementia is now thought to involve vascular processes^{84–90,122}, retinal imaging may provide new insights into the microvascular etiology (versus macrovascular etiology) of dementia^{10,35,58,106,108,123} and facilitate our understanding on different dementia subtypes. In addition, as the association between retinal changes and dementia remains inconclusive, this protocol can also be used to further examine the utility of retinal imaging in population screening or diagnosis of dementia.

In terms of clinical research, retinal imaging might potentially be used in clinical settings to facilitate the preclinical diagnosis or risk assessment of dementia, to confirm clinically diagnosed AD, and to monitor the disease progression or response to therapy. The application of retinal imaging in population screening is particularly intriguing as neuronal and microvascular changes, which might be reflected by similar retinal changes, occur much earlier than the appearance of cortical atrophy and cognitive decline^{124,125}. However, the strength of associations between retinal imaging measures and dementia is only modest and several retinal correlates of AD have not been consistently observed^{8,47,48,59,109}. More prospective clinical studies with large cohorts are required to evaluate the clinical utility of retinal imaging in the diagnosis and monitoring of AD.

In terms of the technical aspects of our method, recent advances in retinal imaging techniques, such as the ultra-wide field retinal imaging and the OCT-angiography, may allow us to obtain more information from the retina. The ultra-wide field retinal imaging technology, based on the principle of confocal laser scanning microscopy combined with a concave elliptical mirror, can capture up to 200° of the retina in a single image without pupil dilation^{126,127} and thus allow more extensive assessment of peripheral retinal lesions. It is possible that assessment of more peripheral vessels may provide an even better representation of the overall retinal vasculature¹⁷. It has been reported that the ultra-wide field retinal imaging can achieve satisfactory performance in both vessel segmentation and width estimation. In addition, the invention of OCT-angiography also allows non-dye-based mapping of the retinal capillary network, which might provide more information on microvascular changes related to dementia. In view of image analysis methods, more research is required to explore other state-of-the-art image processing and quantitative methods, such as tree topology estimation¹²⁸, to analyze the images captured by these imaging modalities.

[Place Figure 13 Here]

This protocol describes a non-invasive, quantitative and semi-automated method to study dementia using retinal imaging techniques (**Figure 13**). Considering the accessibility of retinal imaging and its robust associations with the brain, imaging the retina may provide new insights

into pathophysiological processes of dementia occurring in the brain and, potentially, aid in the diagnosis and risk assessment of dementia. However, the associations reported remain controversial and further studies are required to assess the potential utility of retinal imaging. It should also be noted that a thorough clinical evaluation remains essential in the assessment of dementia.

ACKNOWLEDGMENTS:

We would like to express our appreciation to the School of Computing, National University of Singapore for technical support.

DISCLOSURES:

Regarding potential financial ties, the author Tien Y. Wong is a co-inventor of the Singapore I Vessel Assessment (SIVA) program used in this article.

REFERENCES:

1. International, A. D. The prevalence of dementia worldwide. *Alzheimer's Dis. Int.* (December), 1–2, doi:10.1097/00002093-198802040-00015 (2008).
2. Wimo, A., Winblad, B. & Jönsson, L. The worldwide societal costs of dementia: Estimates for 2009. *Alzheimer's Dement.* **6** (2), 98–103, doi:10.1016/j.jalz.2010.01.010 (2010).
3. Comas-Herrera, A., Northey, S., Wittenberg, R., Knapp, M., Bhattacharyya, S. & Burns, A. Future costs of dementia-related long-term care: exploring future scenarios. *Int. Psychogeriatr.* **23** (1), 20–30, doi:10.1017/S1041610210000025 (2011).
4. Association, A. 2014 Alzheimer's disease facts and figures. *Alzheimer's Dement.* **10** (2), e47–e92, doi:10.1016/j.jalz.2014.02.001 (2014).
5. Prince, M., Bryce, R., Albanese, E., Wimo, A., Ribeiro, W. & Ferri, C. P. The global prevalence of dementia: a systematic review and metaanalysis. *Alzheimer's Dement.* **9** (1), 63–75.e2, doi:10.1016/j.jalz.2012.11.007 (2013).
6. 2016 Alzheimer's disease facts and figures. *Alzheimer's Dement.* **12** (4), 459–509, doi:10.1016/j.jalz.2016.03.001 (2016).
7. Asih, P. R., Chatterjee, P., Verdile, G., Gupta, V. B., Trengove, R. D. & Martins, R. N. Clearing the amyloid in Alzheimer's: progress towards earlier diagnosis and effective treatments - an update for clinicians. *Neurodegener. Dis. Manag.* **4** (5), 363–378, doi:10.2217/nmt.14.29 (2014).
8. Cheung, C. Y., Ikram, M. K., Chen, C. & Wong, T. Y. Imaging retina to study dementia and stroke. *Prog. Retin. Eye Res.*, doi:10.1016/j.preteyeres.2017.01.001 (2017).
9. Patton, N., Aslam, T., Macgillivray, T., Pattie, A., Deary, I. J. & Dhillon, B. Retinal vascular image analysis as a potential screening tool for cerebrovascular disease: a rationale based on homology between cerebral and retinal microvasculatures. *J. Anat.* **206** (4), 319–48, doi:10.1111/j.1469-7580.2005.00395.x (2005).
10. London, A., Benhar, I. & Schwartz, M. The retina as a window to the brain-from eye research to CNS disorders. *Nat. Rev. Neurol.* **9** (1), 44–53, doi:10.1038/nrneurol.2012.227 (2013).
11. Crowe, M. J., Bresnahan, J. C., Shuman, S. L., Masters, J. N. & Beattie, M. S. Apoptosis and delayed degeneration after spinal cord injury in rats and monkeys. *Nat Med* **3** (1), 73–76, doi:10.1038/nm0197-73 (1997).

12. Levkovitch-Verbin, H., Quigley, H. A., Kerrigan-Baumrind, L. A., D'Anna, S. A., Kerrigan, D. & Pease, M. E. Optic nerve transection in monkeys may result in secondary degeneration of retinal ganglion cells. *Investig. Ophthalmol. Vis. Sci.* **42** (5), 975–982 (2001).
13. Levkovitch-Verbin, H., Quigley, H. A., Martin, K. R., Zack, D. J., Pease, M. E. & Valenta, D. F. A model to study differences between primary and secondary degeneration of retinal ganglion cells in rats by partial optic nerve transection. *Invest Ophthalmol Vis Sci* **44** (8), 3388–3393., doi:10.1167/iovs.02-0646 (2003).
14. Yoles, E. & Schwartz, M. Degeneration of spared axons following partial white matter lesion: implications for optic nerve neuropathies. *Exp Neurol* **153** (1), 1–7, doi:10.1006/exnr.1998.6811 (1998).
15. Sadun, A. A., Borchert, M., DeVita, E., Hinton, D. R. & Bassi, C. J. Assessment of Visual Impairment in Patients With Alzheimer's Disease. *Am. J. Ophthalmol.* **104** (2), 113–120, doi:10.1016/0002-9394(87)90001-8 (1987).
16. Schlotterer, G., Moscovitch, M. & Crapper-Mclachlan, D. Visual processing deficits as assessed by spatial frequency contrast sensitivity and backward masking in normal ageing and alzheimer's disease. *Brain* **107** (1), 309–324, doi:10.1093/brain/107.1.309 (1984).
17. Cheung, C. Y. L. *et al.* A new method to measure peripheral retinal vascular caliber over an extended area. *Microcirculation* **17** (7), 495–503, doi:10.1111/j.1549-8719.2010.00048.x (2010).
18. Knudtson, M. D., Lee, K. E., Hubbard, L. D., Wong, T. Y., Klein, R. & Klein, B. E. K. Revised formulas for summarizing retinal vessel diameters. *Curr. Eye Res.* **27** (3), 143–149, doi:10.1076/ceyr.27.3.143.16049 (2003).
19. Hubbard, L. D. *et al.* Methods for evaluation of retinal microvascular abnormalities associated with hypertension/sclerosis in the Atherosclerosis Risk in Communities Study. *Ophthalmology* **106** (12), 2269–2280, doi:10.1016/S0161-6420(99)90525-0 (1999).
20. Patton, N. *et al.* The association between retinal vascular network geometry and cognitive ability in an elderly population. *Investig. Ophthalmol. Vis. Sci.* **48** (5), 1995–2000, doi:10.1167/iovs.06-1123 (2007).
21. VanHecke, M. V. *et al.* Are retinal microvascular abnormalities associated with large artery endothelial dysfunction and intima-media thickness? The Hoorn Study. *Clin. Sci. London Engl.* **1979** **110** (5), 597–604, doi:10.1042/CS20050270 (2006).
22. Tien, Y. W. *et al.* Retinal vascular caliber, cardiovascular risk factors, and inflammation: The Multi-Ethnic Study of Atherosclerosis (MESA). *Investig. Ophthalmol. Vis. Sci.* **47** (6), 2341–2350, doi:10.1167/iovs.05-1539 (2006).
23. Leung, H. *et al.* Relationships between age, blood pressure, and retinal vessel diameters in an older population. *Investig. Ophthalmol. Vis. Sci.* **44** (7), 2900–2904, doi:10.1167/iovs.02-1114 (2003).
24. Wong, T. Y. *et al.* The prevalence and risk factors of retinal microvascular abnormalities in older persons: The cardiovascular health study. *Ophthalmology* **110** (4), 658–666, doi:10.1016/S0161-6420(02)01931-0 (2003).
25. Ikram, M. K. *et al.* Retinal vessel diameters and risk of stroke: The Rotterdam Study. *Neurology* **66** (9), 1339–1343, doi:10.1212/01.wnl.0000210533.24338.ea (2006).
26. Wong, T. Y., Knudtson, M. D., Klein, R., Klein, B. E. K., Meuer, S. M. & Hubbard, L. D. Computer-assisted measurement of retinal vessel diameters in the Beaver Dam Eye Study:

- Methodology, correlation between eyes, and effect of refractive errors. *Ophthalmology* **111** (6), 1183–1190, doi:10.1016/j.ophtha.2003.09.039 (2004).
27. Sasongko, M. B. *et al.* Alterations in retinal microvascular geometry in young type 1 diabetes. *Diabetes Care* **33** (6), 1331–1336, doi:10.2337/dc10-0055 (2010).
 28. Cheung, C. Y.-L. *et al.* Retinal vascular tortuosity, blood pressure, and cardiovascular risk factors. *Ophthalmology* **118** (5), 812–8, doi:10.1016/j.ophtha.2010.08.045 (2011).
 29. Mainster, M. a The fractal properties of retinal vessels: embryological and clinical implications. *Eye* **4** (Pt 1) (1), 235–241, doi:10.1038/eye.1990.33 (1990).
 30. Liew, G. *et al.* The Retinal Vasculature as a Fractal: Methodology, Reliability, and Relationship to Blood Pressure. *Ophthalmology* **115** (11), doi:10.1016/j.ophtha.2008.05.029 (2008).
 31. Stosic, T. & Stosic, B. D. Multifractal analysis of human retinal vessels. *IEEE Trans. Med. Imaging* **25** (8), 1101–1107, doi:10.1109/TMI.2006.879316 (2006).
 32. Zamir, M., Medeiros, J. a, Cunningham, T. K. & M. Zamir, J. A. Medeiros, T. K. C. Arterial bifurcations in the human retina. *J. Gen. Physiol.* **74** (4), 537–48, doi:10.1085/jgp.74.4.537 (1979).
 33. Mwanza, J. C., Oakley, J. D., Budenz, D. L., Chang, R. T., Knight, O. J. & Feuer, W. J. Macular ganglion cell-inner plexiform layer: Automated detection and thickness reproducibility with spectral domain-optical coherence tomography in glaucoma. *Investig. Ophthalmol. Vis. Sci.* **52** (11), 8323–8329, doi:10.1167/iovs.11-7962 (2011).
 34. Bendschneider, D. *et al.* Retinal nerve fiber layer thickness in normals measured by spectral domain OCT. *J. Glaucoma* **19** (7), 475–482, doi:10.1097/IJG.0b013e3181c4b0c7 (2010).
 35. Cheung, C. Y., Ong, Y.-T., Ikram, M. K., Chen, C. & Wong, T. Y. Retinal Microvasculature in Alzheimer's Disease. *J. Alzheimer's Dis.* **42** (s4), S339–S352, doi:10.3233/JAD-141596 (2014).
 36. Murray, C. D. THE PHYSIOLOGICAL PRINCIPLE OF MINIMUM WORK APPLIED TO THE ANGLE OF BRANCHING OF ARTERIES. *J. Gen. Physiol.* (4), 835–841, doi:10.1103/PhysRevC.71.064610 (1926).
 37. Ding, J. *et al.* Early retinal arteriolar changes and peripheral neuropathy in diabetes. *Diabetes Care* **35** (5), 1098–1104, doi:10.2337/dc11-1341 (2012).
 38. Yim, C. *et al.* Retinal Ganglion Cell Analysis Using High-Definition Optical Coherence Tomography in Patients with Mild Cognitive Impairment and Alzheimer's Disease. *J. Alzheimer's Dis. Retin. Ganglion Cell Anal. MCI AD* **45** (1), 45–56, doi:10.3233/JAD-141659 (2015).
 39. Stein, D. M., Wollstein, G., Ishikawa, H., Hertzmark, E., Noecker, R. J. & Schuman, J. S. Effect of Corneal Drying on Optical Coherence Tomography. *Ophthalmology* **113** (6), 985–991, doi:10.1016/j.ophtha.2006.02.018 (2006).
 40. Mwanza, J. C. *et al.* Effect of Cataract and its Removal on Signal Strength and Peripapillary Retinal Nerve Fiber Layer Optical Coherence Tomography Measurements. *J. Glaucoma* **20** (1), 37–43, doi:10.1097/IJG.0b013e3181ccb93b (2011).
 41. Garcia-Martin, E. *et al.* Influence of cataract surgery on optical coherence tomography and neurophysiology measurements in patients with retinitis pigmentosa. *Am. J. Ophthalmol.* **156** (2), doi:10.1016/j.ajo.2013.03.019 (2013).
 42. Kok, P. H. B. *et al.* The relationship between the optical density of cataract and its influence on retinal nerve fibre layer thickness measured with spectral domain optical coherence tomography. *Acta Ophthalmol.* , doi:10.1111/j.1755-3768.2012.02514.x (2012).
 43. Kim, N. R. *et al.* Influence of cataract on time domain and spectral domain optical

- coherence tomography retinal nerve fiber layer measurements. *J. Glaucoma* **21** (2), 116–22, doi:10.1097/IJG.0b013e31820277da (2012).
44. Hwang, Y. H. & Kim, Y. Y. Effect of Peripapillary Vitreous Opacity on Retinal Nerve Fiber Layer Thickness Measurement Using Optical Coherence Tomography. *Arch. Ophthalmol.* **130** (6), 789–792, doi:10.1001/archophthalmol.2011.2517 (2012).
 45. Schwartz, S. G., Flynn, H. W. & Fisher, Y. L. “Floater scotoma” demonstrated on spectral-domain optical coherence tomography and caused by vitreous opacification. *Ophthalmic Surg. Lasers Imaging Retina* **44** (4), 415–8, doi:10.3928/23258160-20130715-14 (2013).
 46. DeJong, F. J. *et al.* Retinal vascular caliber and risk of dementia: The Rotterdam Study. *Neurology* **76** (9), 816–821, doi:10.1212/WNL.0b013e31820e7baa (2011).
 47. Frost, S. *et al.* Retinal vascular biomarkers for early detection and monitoring of Alzheimer’s disease. *Transl. Psychiatry* **3** (2), e233, doi:10.1038/tp.2012.150 (2013).
 48. Cheung, C. Y. *et al.* Microvascular network alterations in the retina of patients with Alzheimer’s disease. *Alzheimer’s Dement.* **10** (2), 135–142, doi:10.1016/j.jalz.2013.06.009 (2014).
 49. Cheung, C. Y. *et al.* Quantitative and qualitative retinal microvascular characteristics and blood pressure. *J. Hypertens.* **29** (7), 1380–1391, doi:10.1097/HJH.0b013e328347266c (2011).
 50. Cheung, C. Y. *et al.* Retinal vascular fractal dimension and its relationship with cardiovascular and ocular risk factors. *Am. J. Ophthalmol.* **154** (4), 663–674, doi:10.1016/j.ajo.2012.04.016 (2012).
 51. Cheung, C. Y.-L. *et al.* Retinal vascular tortuosity, blood pressure, and cardiovascular risk factors. *Ophthalmology* **118** (5), 812–8, doi:10.1016/j.ophtha.2010.08.045 (2011).
 52. Grinton, M. E. *et al.* The association between retinal vessel morphology and retinal nerve fiber layer thickness in an elderly population. *Ophthalmic Surg. Lasers Imaging* **43** (6 Suppl), S61–6, doi:10.3928/15428877-20120802-03 (2012).
 53. Hughes, A. D. *et al.* Quantification of topological changes in retinal vascular architecture in essential and malignant hypertension. *J. Hypertens.* **24** (5), 889–94, doi:10.1097/01.hjh.0000222759.61735.98 (2006).
 54. Hughes, A. D. *et al.* Determinants of retinal microvascular architecture in normal subjects. *Microcirculation* **16** (2), 159–66, doi:10.1080/10739680802353868 (2009).
 55. Lau, Q. P., Lee, M. L., Hsu, W. & Wong, T. Y. The Singapore Eye Vessel Assessment System. *Image Anal. Model. Ophthalmol.* , 143–160, doi:10.1201/b16510-9 (2014).
 56. Thomas, G. N. *et al.* Measurement of Macular Fractal Dimension Using a Computer-Assisted Program. *Investig. Ophthalmology Vis. Sci.* **55** (4), 2237, doi:10.1167/iovs.13-13315 (2014).
 57. Murray, C. D. The physiological principle of minimal work. I. The vascular system and the cost of blood volume. *Proc. Natl. Acad. Sci.* **12**, 207–214, doi:10.1085/jgp.9.6.835 (1926).
 58. Cheung, C., Chen, C. & Wong, T. Ocular Fundus Photography as a Tool to Study Stroke and Dementia. *Semin. Neurol.* **35** (5), 481–490, doi:10.1055/s-0035-1563570 (2015).
 59. Williams, M. A. *et al.* Retinal microvascular network attenuation in Alzheimer’s disease. *Alzheimer’s Dement. Diagnosis, Assess. Dis. Monit.* **1** (2), 229–235, doi:10.1016/j.dadm.2015.04.001 (2015).
 60. Cheung, C. Y. *et al.* Retinal Vascular Fractal Dimension Is Associated with Cognitive Dysfunction. *J. Stroke Cerebrovasc. Dis.* **23** (1), 43–50, doi:10.1016/j.jstrokecerebrovasdis.2012.09.002 (2014).

61. Hammes, H.-P. *et al.* Diabetic retinopathy: targeting vasoregression. *Diabetes* **60** (1), 9–16, doi:10.2337/db10-0454 (2011).
62. Cheung, C. Y. *et al.* Microvascular network alterations in the retina of patients with Alzheimer's disease. *Alzheimer's Dement.* **10** (2), 135–142, doi:10.1016/j.jalz.2013.06.009 (2014).
63. Frame, M. D. & Sarelius, I. H. Arteriolar bifurcation angles vary with position and when flow is changed. *Microvasc Res* **46** (2), 190–205, doi:10.1006/mvre.1993.1046 (1993).
64. Djonov, V., Baum, O. & Burri, P. H. Vascular remodeling by intussusceptive angiogenesis. *Cell Tissue Res.* **314** (1), 107–117, doi:10.1007/s00441-003-0784-3 (2003).
65. Griffith, T. M. & Edwards, D. H. Basal EDRF activity helps to keep the geometrical configuration of arterial bifurcations close to the Murray optimum. *J. Theor. Biol.* **146** (4), 545–73, doi:10.1016/S0022-5193(05)80378-9 (1990).
66. Griffith, T. M., Edwards, D. H. & Randall, M. D. Blood flow and optimal vascular topography: role of the endothelium. *Basic Res. Cardiol.* **86 Suppl 2**, 89–96, doi:10.1007/978-3-642-72461-9_10 (1991).
67. Chapman, N., Haimes, G., Stanton, A. V., Thom, S. A. M. & Hughes, A. D. Acute effects of oxygen and carbon dioxide on retinal vascular network geometry in hypertensive and normotensive subjects. *Clin. Sci.* **99** (6), 483–8, doi:10.1042/cs0990483 (2000).
68. Heringa, S. M., Bouvy, W. H., van den Berg, E., Moll, A. C., Jaap Kappelle, L. & Jan Biessels, G. Associations between retinal microvascular changes and dementia, cognitive functioning, and brain imaging abnormalities: a systematic review. *J. Cereb. blood flow Metab.* **33** (7), 983–995, doi:10.1038/jcbfm.2013.58 (2013).
69. Ding, J. *et al.* Diabetic retinopathy and cognitive decline in older people with type 2 diabetes: The Edinburgh type 2 diabetes study. *Diabetes* **59** (11), 2883–2889, doi:10.2337/db10-0752 (2010).
70. Parisi, V., Restuccia, R., Fattapposta, F., Mina, C., Bucci, M. G. & Pierelli, F. Morphological and functional retinal impairment in Alzheimer's disease patients. *Clin. Neurophysiol.* **112** (10), 1860–1867, doi:10.1016/S1388-2457(01)00620-4 (2001).
71. Paquet, C., Boissonnot, M., Roger, F., Dighiero, P., Gil, R. & Hugon, J. Abnormal retinal thickness in patients with mild cognitive impairment and Alzheimer's disease. *Neurosci. Lett.* **420** (2), 97–99, doi:http://dx.doi.org/10.1016/j.neulet.2007.02.090 (2007).
72. Moschos, M. M. *et al.* Structural and functional impairment of the retina and optic nerve in Alzheimer's disease. *Curr. Alzheimer Res.* **9** (7), 782–788, doi:10.2174/156720512802455340 (2012).
73. Lu, Y. *et al.* Retinal nerve fiber layer structure abnormalities in early Alzheimer's disease: Evidence in optical coherence tomography. *Neurosci. Lett.* **480** (1), 69–72, doi:10.1016/j.neulet.2010.06.006 (2010).
74. Kesler, A., Vakhapova, V., Korczyn, A. D., Naftaliev, E. & Neudorfer, M. Retinal thickness in patients with mild cognitive impairment and Alzheimer's disease. *Clin. Neurol. Neurosurg.* **113** (7), 523–526, doi:10.1016/j.clineuro.2011.02.014 (2011).
75. Ascaso, F. J. *et al.* Retinal alterations in mild cognitive impairment and Alzheimer's disease: An optical coherence tomography study. *J. Neurol.* **261** (8), 1522–1530, doi:10.1007/s00415-014-7374-z (2014).
76. Berisha, F., Feke, G. T., Trempe, C. L., McMeel, J. W. & Schepens, C. L. Retinal abnormalities in early Alzheimer's disease. *Investig. Ophthalmol. Vis. Sci.* **48** (5), 2285–2289,

doi:10.1167/iovs.06-1029 (2007).

77. Iseri, P. K., Altina??, ??zg??l, Tokay, T. &Y??ksel, N. Relationship between Cognitive Impairment and Retinal Morphological and Visual Functional Abnormalities in Alzheimer Disease. *J. Neuro-Ophthalmology* **26** (1), 18–24, doi:10.1097/01.wno.0000204645.56873.26 (2006).
78. Garcia-Martin, E. S. *et al.* Macular thickness as a potential biomarker of mild Alzheimer's disease. *Ophthalmology* **121** (5), 1149–1151.e3, doi:10.1016/j.ophtha.2013.12.023 (2014).
79. Ko, F. *et al.* Retinal Nerve Fiber Layer Thinning Associated With Poor Cognitive Function Among A Large Cohort, The Uk Biobank. *Alzheimer's Dement.* **12** (7), P317–P318, doi:10.1016/j.jalz.2016.06.575 (2016).
80. Moreno-Ramos, T., Benito-Leon, J., Villarejo, A. &Bermejo-Pareja, F. Retinal nerve fiber layer thinning in dementia associated with Parkinson's disease, dementia with Lewy bodies, and Alzheimer's disease. *J. Alzheimers. Dis.* **34** (3), 659–664, doi:10.3233/JAD-121975 (2013).
81. Moschos, M. M. *et al.* Morphologic changes and functional retinal impairment in patients with Parkinson disease without visual loss. *Eur. J. Ophthalmol.* **21** (1), 24–29, doi:10.5301/EJO.2010.1318 (2011).
82. Garcia-Martin, E. *et al.* Ability and reproducibility of Fourier-domain optical coherence tomography to detect retinal nerve fiber layer atrophy in Parkinson's disease. *Ophthalmology* **119** (10), 2161–2167, doi:10.1016/j.ophtha.2012.05.003 (2012).
83. Yip, W. *et al.* Comparison of Common Retinal Vessel Caliber Measurement Software and a Conversion Algorithm. *Transl. Vis. Sci. Technol.* **5** (5), 11, doi:10.1167/tvst.5.5.11 (2016).
84. Gorelick, P. B. *et al.* Vascular contributions to cognitive impairment and dementia: a statement for healthcare professionals from the american heart association/american stroke association. *Stroke*. **42** (9), 2672–2713, doi:10.1161/STR.0b013e3182299496 (2011).
85. Brown, W. R. &Thore, C. R. Review: Cerebral microvascular pathology in ageing and neurodegeneration. *Neuropathol. Appl. Neurobiol.* **37** (1), 56–74, doi:10.1111/j.1365-2990.2010.01139.x (2011).
86. DeSilva, T. M. &Faraci, F. M. Microvascular Dysfunction and Cognitive Impairment. *Cell. Mol. Neurobiol.* **36** (2), 241–258, doi:10.1007/s10571-015-0308-1 (2016).
87. Kalaria, R. N., Akinyemi, R. &Ihara, M. Does vascular pathology contribute to Alzheimer changes? *J. Neurol. Sci.* **322** (1–2), 141–147, doi:10.1016/j.jns.2012.07.032 (2012).
88. Kling, M. A., Trojanowski, J. Q., Wolk, D. A., Lee, V. M. Y. &Arnold, S. E. Vascular disease and dementias: paradigm shifts to drive research in new directions. *Alzheimers. Dement.* **9** (1), 76–92, doi:10.1016/j.jalz.2012.02.007 (2013).
89. O'Brien, J. T. *et al.* Vascular cognitive impairment. *Lancet Neurol.* **2** (2), 89–98, doi:10.1016/S1474-4422(03)00305-3 (2003).
90. Chen, C. *et al.* Alzheimer's disease with cerebrovascular disease: current status in the Asia-Pacific region. *J. Intern. Med.* **280** (4), 359–374, doi:10.1111/joim.12495 (2016).
91. Pérez, M. A., Bruce, B. B., Newman, N. J. &Biousse, V. The use of retinal photography in nonophthalmic settings and its potential for neurology. *Neurologist* **18** (6), 350–5, doi:10.1097/NRL.0b013e318272f7d7 (2012).
92. Boppart, S. A. Optical coherence tomography: Technology and applications for neuroimaging. *Psychophysiology* **40** (4), 529–541, doi:10.1111/1469-8986.00055 (2003).
93. Hee, M. R. *et al.* Optical coherence tomography of the human retina. *Arch. Ophthalmol.* **113** (3), 325–32, doi:10.1001/archophth.1995.01100030081025 (1995).

94. Huang, D. *et al.* Optical coherence tomography. *Science* (80-.). **254** (5035), 1178–81, doi:10.1126/science.1957169 (1991).
95. vanVelthoven, M. E. J., Verbraak, F. D., Yannuzzi, L., Rosen, R. B., Podoleanu, A. G. H. & deSmet, M. D. Imaging the retina by en face optical coherence tomography. *Retina* **26** (2), 129–136, doi:10.1097/00006982-200602000-00001 (2006).
96. Costa, R. A. *et al.* Retinal assessment using optical coherence tomography. *Prog. Retin. Eye Res.* **25** (3), 325–353, doi:10.1016/j.preteyeres.2006.03.001 (2006).
97. DeBuc, D. C., Somfai, G. M., Ranganathan, S., Tátrai, E., Ferencz, M. & Puliafito, C. A. Reliability and reproducibility of macular segmentation using a custom-built optical coherence tomography retinal image analysis software. *J. Biomed. Opt.* **14** (6), 64023, doi:10.1117/1.3268773 (2009).
98. Budenz, D. L. *et al.* Determinants of Normal Retinal Nerve Fiber Layer Thickness Measured by Stratus OCT. *Ophthalmology* **114** (6), 1046–1052, doi:10.1016/j.ophtha.2006.08.046 (2007).
99. Leung, C. K. S. *et al.* Retinal Nerve Fiber Layer Imaging with Spectral-Domain Optical Coherence Tomography: A Prospective Analysis of Age-Related Loss. *Ophthalmology* **119** (4), 731–737, doi:10.1016/j.ophtha.2011.10.010 (2012).
100. Cettomai, D. *et al.* Reproducibility of optical coherence tomography in multiple sclerosis. *Arch. Neurol.* **65** (9), 1218–1222, doi:10.1001/archneur.65.9.1218; 10.1001/archneur.65.9.1218 (2008).
101. Garcia-Martin, E., Pinilla, I., Idoipe, M., Fuertes, I. & Pueyo, V. Intra and interoperator reproducibility of retinal nerve fibre and macular thickness measurements using Cirrus Fourier-domain OCT. *Acta Ophthalmol.* **89** (1), doi:10.1111/j.1755-3768.2010.02045.x (2011).
102. Garcia-Martin, E., Pueyo, V., Pinilla, I., Ara, J.-R., Martin, J. & Fernandez, J. Fourier-domain OCT in multiple sclerosis patients: reproducibility and ability to detect retinal nerve fiber layer atrophy. *Invest. Ophthalmol. Vis. Sci.* **52** (7), 4124–31, doi:10.1167/iovs.10-6643 (2011).
103. Menke, M. N., Knecht, P., Sturm, V., Dabov, S. & Funk, J. Reproducibility of nerve fiber layer thickness measurements using 3D fourier-domain OCT. *Invest. Ophthalmol. Vis. Sci.* **49** (12), 5386–91, doi:10.1167/iovs.07-1435 (2008).
104. Mwanza, J. C. *et al.* Reproducibility of peripapillary retinal nerve fiber layer thickness and optic nerve head parameters measured with cirrus HD-OCT in glaucomatous eyes. *Investig. Ophthalmol. Vis. Sci.* **51** (11), 5724–5730, doi:10.1167/iovs.10-5222 (2010).
105. Syc, S. B. *et al.* Reproducibility of high-resolution optical coherence tomography in multiple sclerosis. *Mult Scler* **16** (7), 829–839, doi:10.1177/1352458510371640\1352458510371640 [pii] (2010).
106. Ikram, M. K., Cheung, C. Y., Wong, T. Y. & Chen, C. P. L. H. Retinal pathology as biomarker for cognitive impairment and Alzheimer's disease. *J. Neurol. Neurosurg. Psychiatry* **83** (9), 917–22, doi:10.1136/jnnp-2011-301628 (2012).
107. MacGillivray, T. J., Trucco, E., Cameron, J. R., Dhillon, B., Houston, J. G. & vanBeek, E. J. R. Retinal imaging as a source of biomarkers for diagnosis, characterization and prognosis of chronic illness or long-term conditions. *Br. J. Radiol.* **87** (1040), 20130832, doi:10.1259/bjr.20130832 (2014).
108. Patton, N. *et al.* Retinal image analysis: Concepts, applications and potential. *Prog. Retin. Eye Res.* **25** (1), 99–127, doi:10.1016/j.preteyeres.2005.07.001 (2006).
109. McGrory, S. *et al.* The application of retinal fundus camera imaging in dementia: A

- systematic review. *Alzheimer's Dement. Diagnosis, Assess. Dis. Monit.* **6**, 91–107, doi:10.1016/j.dadm.2016.11.001 (2017).
110. Wong, T. Y., Knudtson, M. D., Klein, R., Klein, B. E. K., Meuer, S. M. & Hubbard, L. D. Computer-assisted measurement of retinal vessel diameters in the Beaver Dam Eye Study: methodology, correlation between eyes, and effect of refractive errors. *Ophthalmology* **111** (6), 1183–90, doi:10.1016/j.ophtha.2003.09.039 (2004).
 111. Hardin, J. S., Taibbi, G., Nelson, S. C., Chao, D. & Vizzeri, G. Factors Affecting Cirrus-HD OCT Optic Disc Scan Quality: A Review with Case Examples. *J. Ophthalmol.* **2015**, 1–16, doi:10.1155/2015/746150 (2015).
 112. Kim, N. R. *et al.* Influence of Cataract on Time Domain and Spectral Domain Optical Coherence Tomography Retinal Nerve Fiber Layer Measurements. *J. Glaucoma* , 1, doi:10.1097/IJG.0b013e31820277da (2010).
 113. Li, H. *et al.* Lens opacity and refractive influences on the measurement of retinal vascular fractal dimension. *Acta Ophthalmol.* **88** (6), e234–e240, doi:10.1111/j.1755-3768.2010.01975.x (2010).
 114. Maberley, D., Morris, A., Hay, D., Chang, A., Hall, L. & Mandava, N. A comparison of digital retinal image quality among photographers with different levels of training using a non-mydratic fundus camera. *Ophthalmic Epidemiol.* **11** (3), 191–7, doi:10.1080/09286580490514496 (2004).
 115. Rochtchina, E., Wang, J. J., Taylor, B., Wong, T. Y. & Mitchell, P. Ethnic variability in retinal vessel caliber: A potential source of measurement error from ocular pigmentation?—The Sydney childhood eye study. *Investig. Ophthalmol. Vis. Sci.* **49** (4), 1362–1366, doi:10.1167/iovs.07-0150 (2008).
 116. Wainwright, A. *et al.* Effect of image quality, color, and format on the measurement of retinal vascular fractal dimension. *Investig. Ophthalmol. Vis. Sci.* **51** (11), 5525–5529, doi:10.1167/iovs.09-4129 (2010).
 117. Nguyen, T. T. & Wong, T. Y. Retinal vascular manifestations of metabolic disorders. *Trends Endocrinol. Metab.* **17** (7), 262–268, doi:10.1016/j.tem.2006.07.006 (2006).
 118. Ding, J. *et al.* Retinal vascular caliber and the development of hypertension: a meta-analysis of individual participant data. *J. Hypertens.* **32** (2), 207–15, doi:10.1097/HJH.0b013e32836586f4 (2014).
 119. Nguyen, T. T. & Wong, T. Y. Retinal vascular changes and diabetic retinopathy. *Curr. Diab. Rep.* **9** (4), 277–283, doi:10.1007/s11892-009-0043-4 (2009).
 120. Leung, C. K. S., Ye, C., Weinreb, R. N., Yu, M., Lai, G. & Lam, D. S. Impact of Age-related Change of Retinal Nerve Fiber Layer and Macular Thicknesses on Evaluation of Glaucoma Progression. *Ophthalmology* **120** (12), 2485–2492, doi:10.1016/j.ophtha.2013.07.021 (2013).
 121. Sherry, L. M. *et al.* Reliability of computer-assisted retinal vessel measurement in a population. *Clin. Experiment. Ophthalmol.* **30** (3), 179–182, doi:10.1046/j.1442-9071.2002.00520.x (2002).
 122. Wardlaw, J. M. *et al.* Neuroimaging standards for research into small vessel disease and its contribution to ageing and neurodegeneration. *Lancet Neurol.* **12** (8), 822–838, doi:10.1016/S1474-4422(13)70124-8 (2013).
 123. Patton, N., Aslam, T., MacGillivray, T., Pattie, A., Deary, I. J. & Dhillon, B. Retinal vascular image analysis as a potential screening tool for cerebrovascular disease: A rationale based on homology between cerebral and retinal microvasculatures. *J. Anat.* **206** (4), 319–348,

doi:10.1111/j.1469-7580.2005.00395.x (2005).

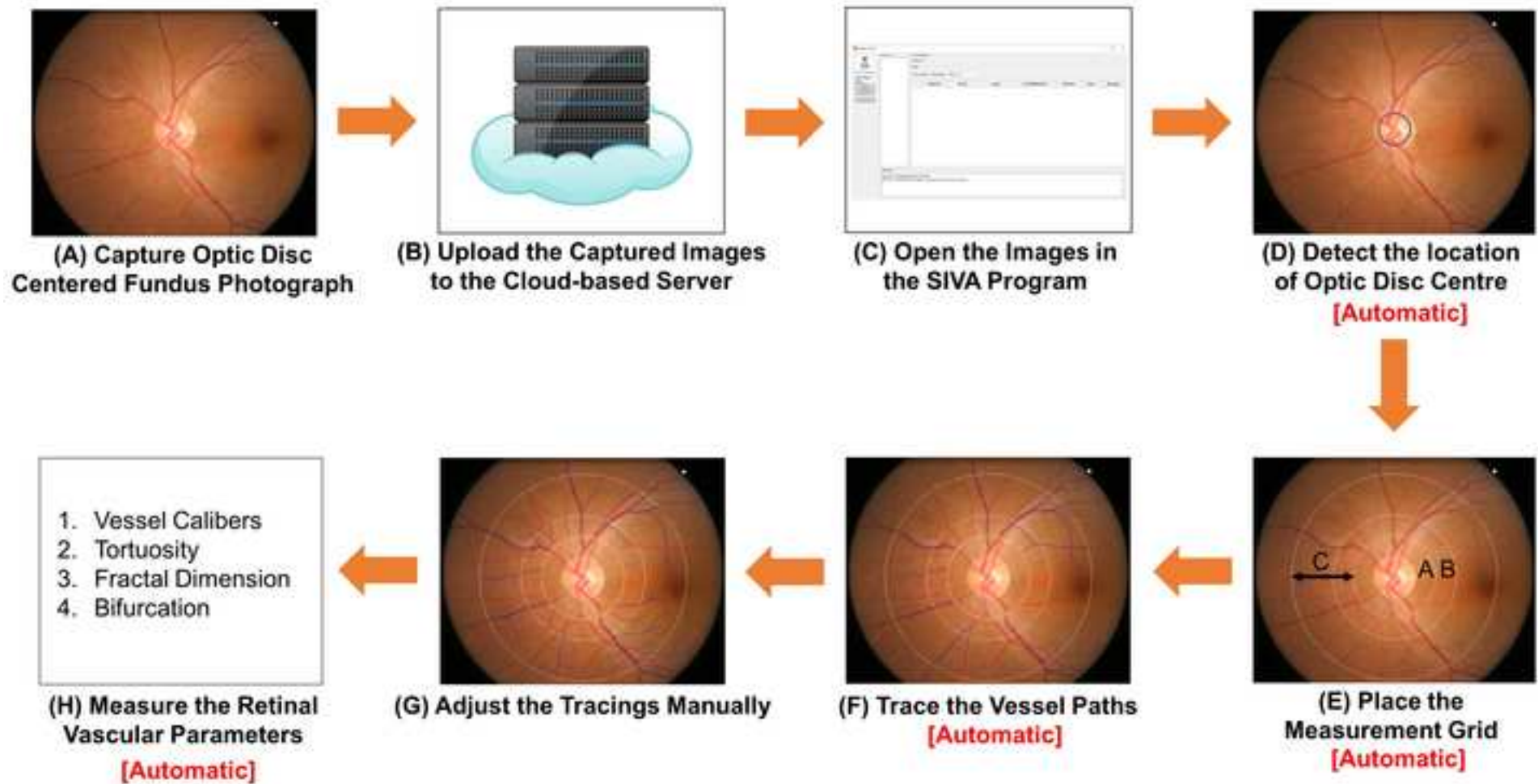
124. Ferri, C. P. *et al.* Global prevalence of dementia: A Delphi consensus study. *Lancet* **366** (9503), 2112–2117, doi:10.1016/S0140-6736(05)67889-0 (2005).

125. Sahadevan, S. *et al.* Ethnic differences in Singapore's dementia prevalence: The stroke, Parkinson's disease, epilepsy, and dementia in Singapore study. *J. Am. Geriatr. Soc.* **56** (11), 2061–2068, doi:10.1111/j.1532-5415.2008.01992.x (2008).

126. Kernt, M. *et al.* Assessment of diabetic retinopathy using nonmydriatic ultra-widefield scanning laser ophthalmoscopy (Optomap) compared with ETDRS 7-field stereo photography. *Diabetes Care* **35** (12), 2459–2463, doi:10.2337/dc12-0346 (2012).

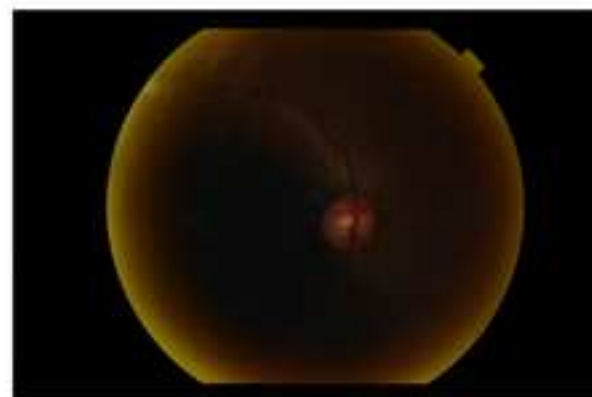
127. Manivannan, A., Plskova, J., Farrow, A., Mckay, S., Sharp, P. F. & Forrester, J.V. Ultra-wide-field fluorescein angiography of the ocular fundus. *Am. J. Ophthalmol.* **140** (3), 525–527, doi:10.1016/j.ajo.2005.02.055 (2005).

128. Estrada, R., Tomasi, C., Schmidler, S. C. & Farsiu, S. Tree topology estimation. *IEEE Trans. Pattern Anal. Mach. Intell.* **37** (8), 1688–1701, doi:10.1109/TPAMI.2014.2382116 (2015).





(A) Optimal Result



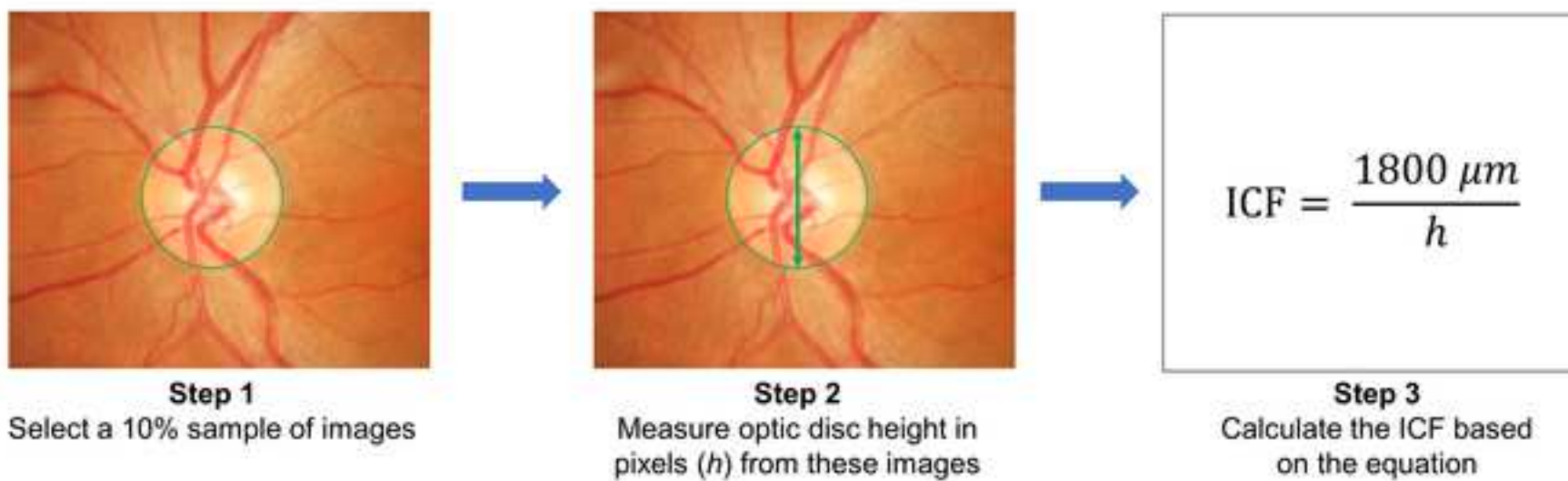
(B) Poor Pupil Dilation

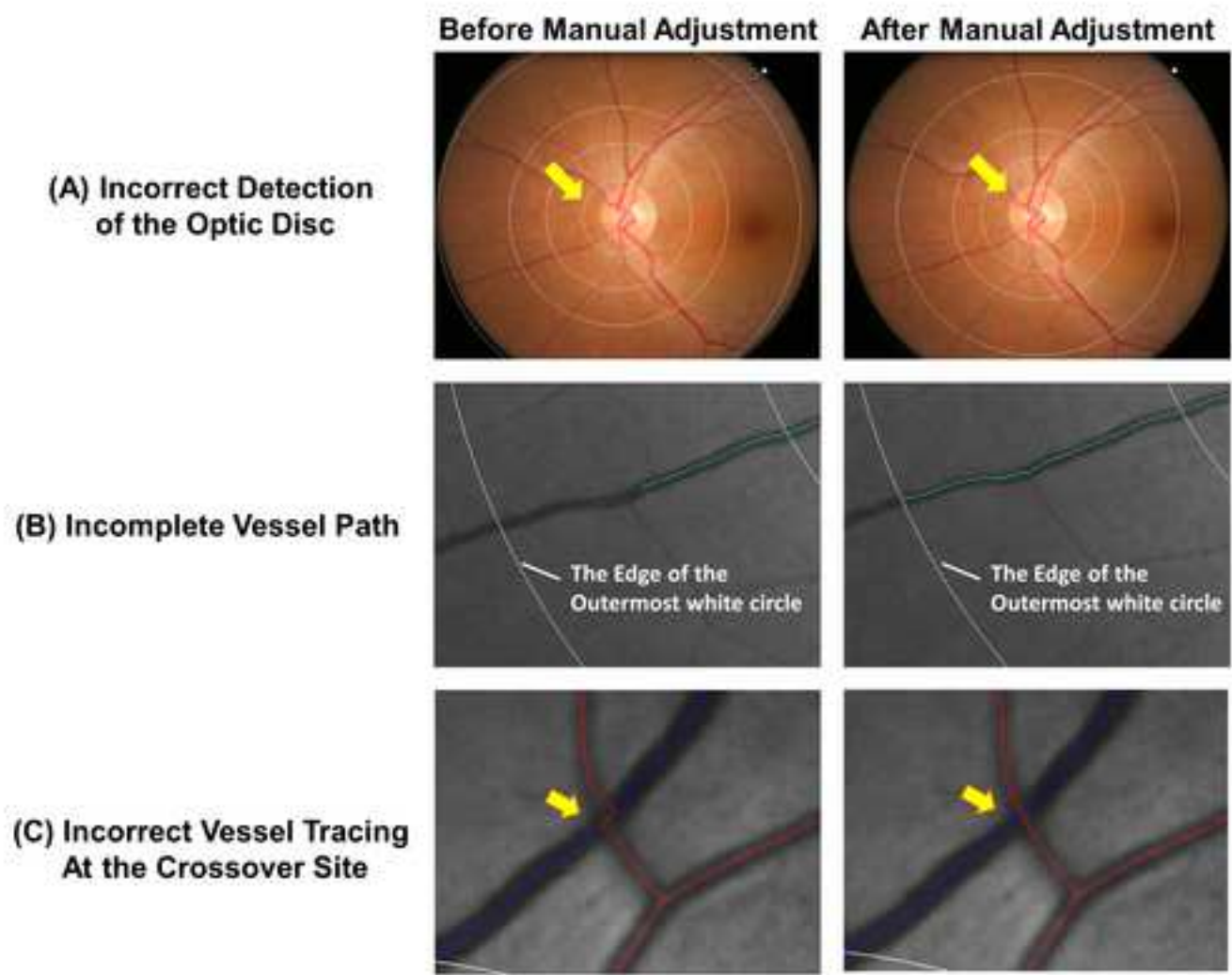


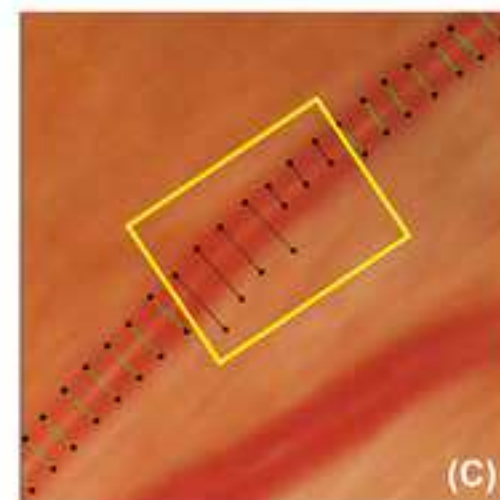
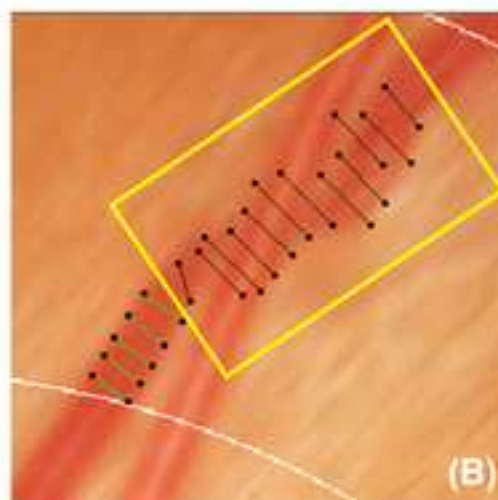
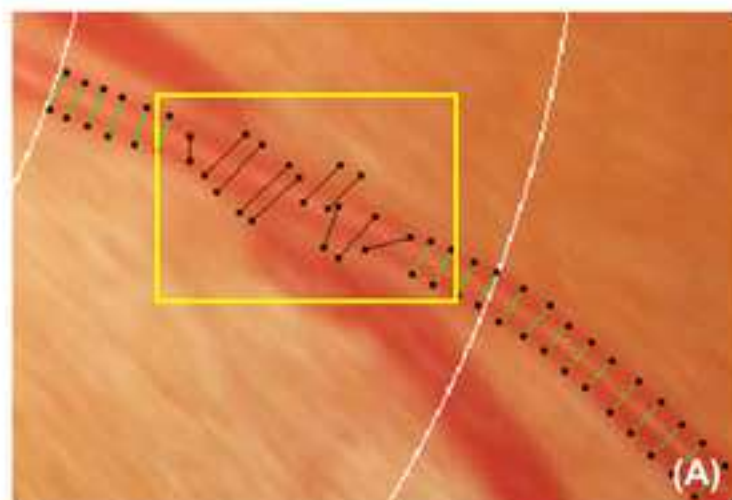
(C) Optic Disc Not Centered

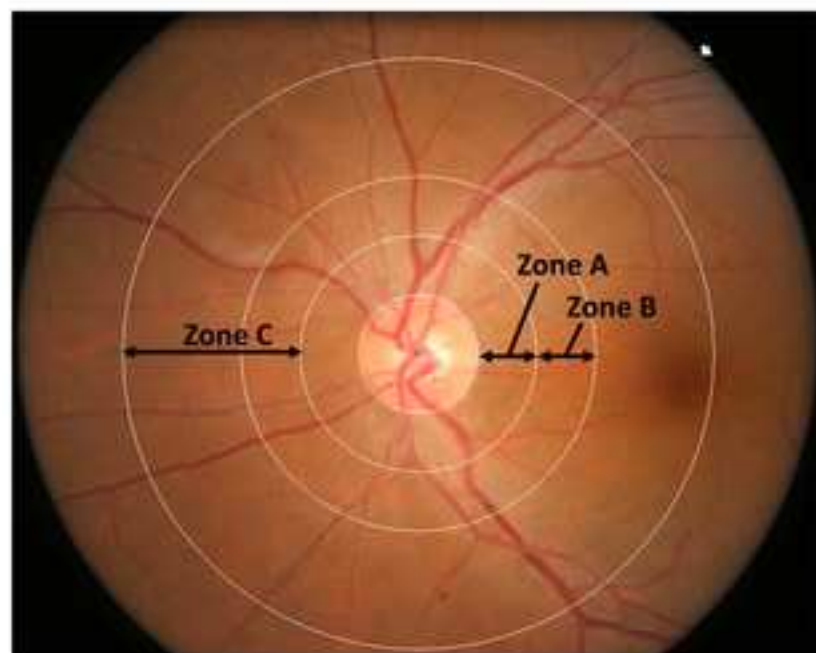


(D) Inaccurate Focus

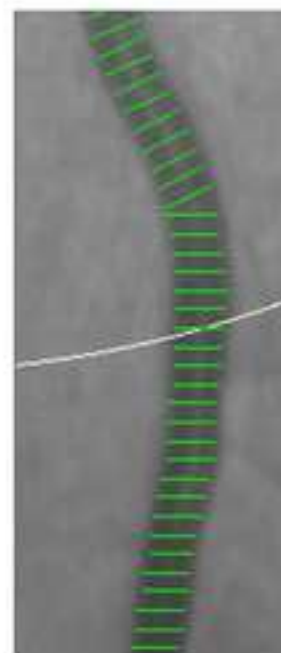




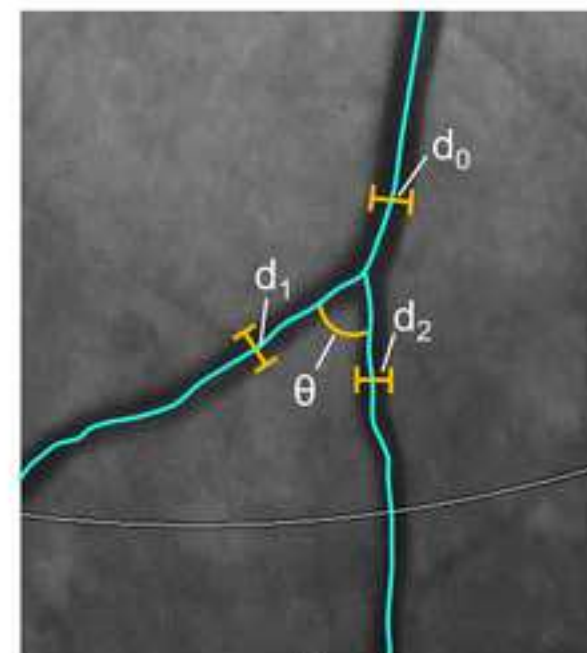




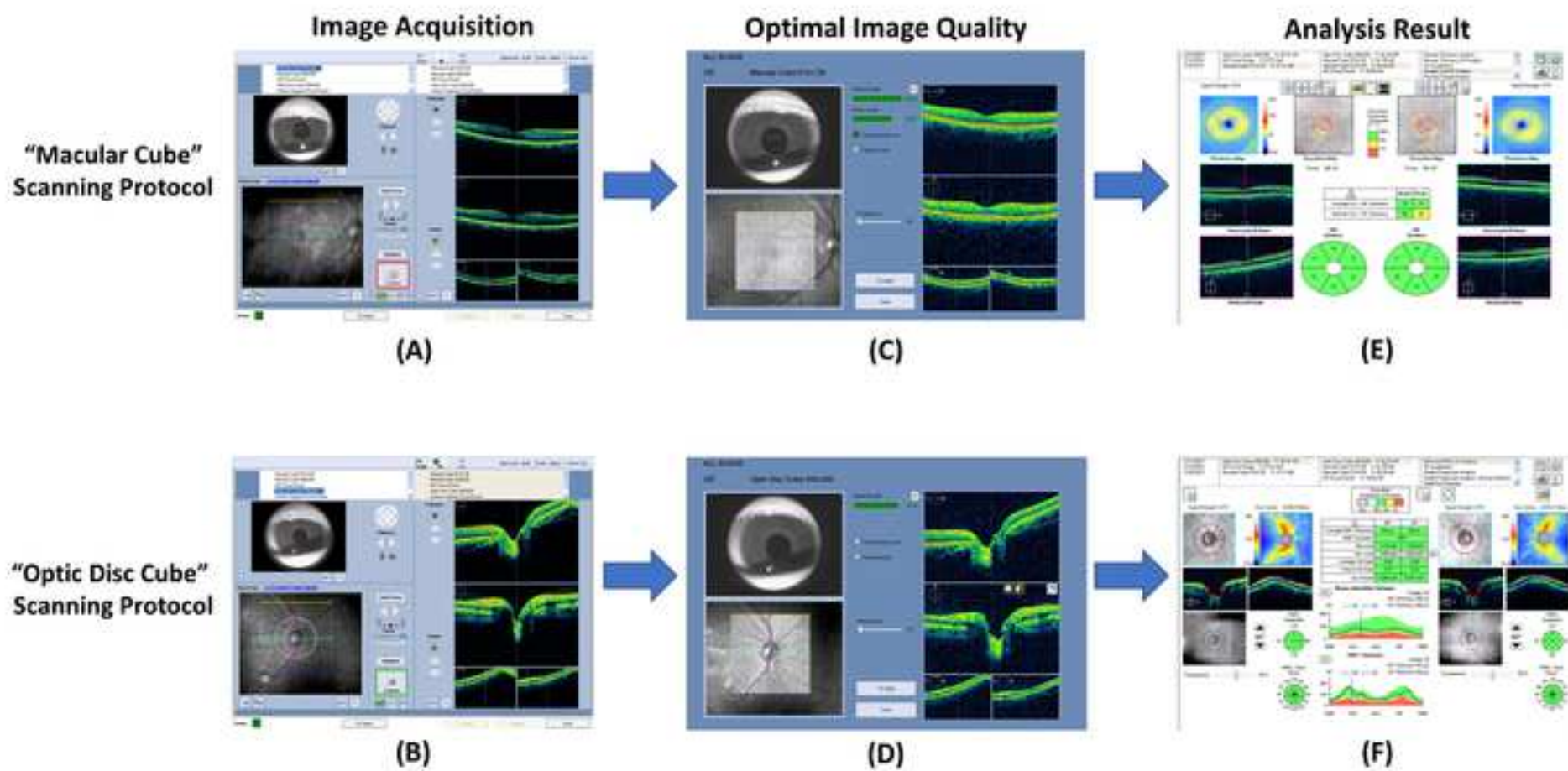
(A)

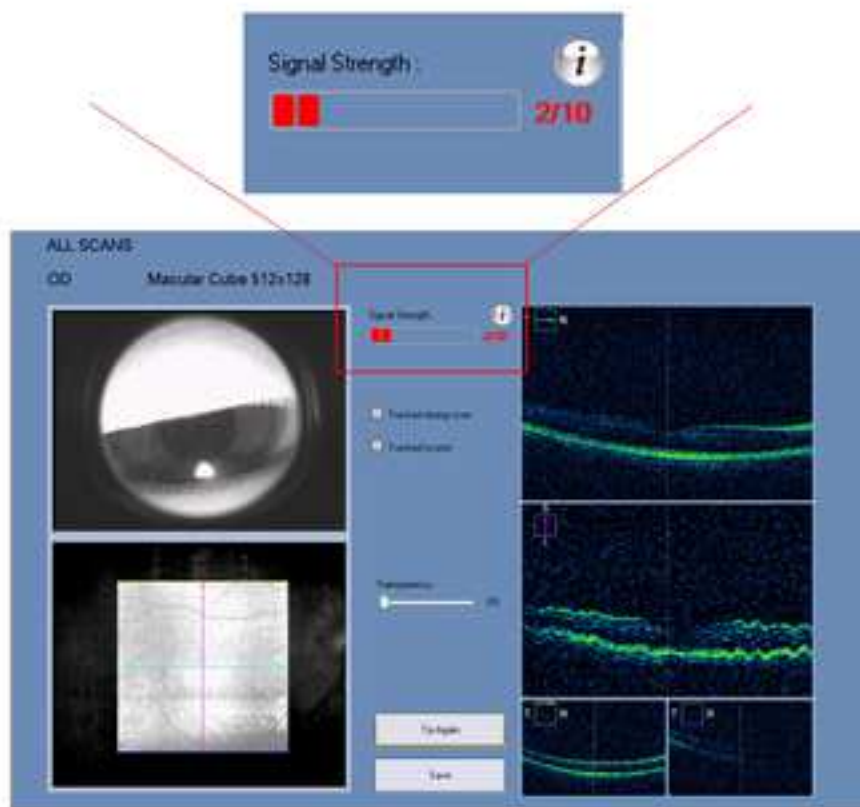


(B)

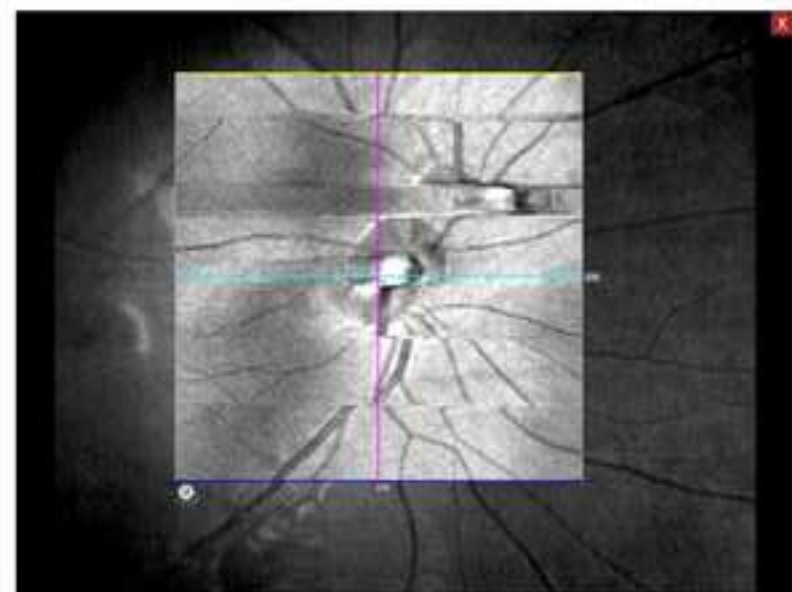


(C)

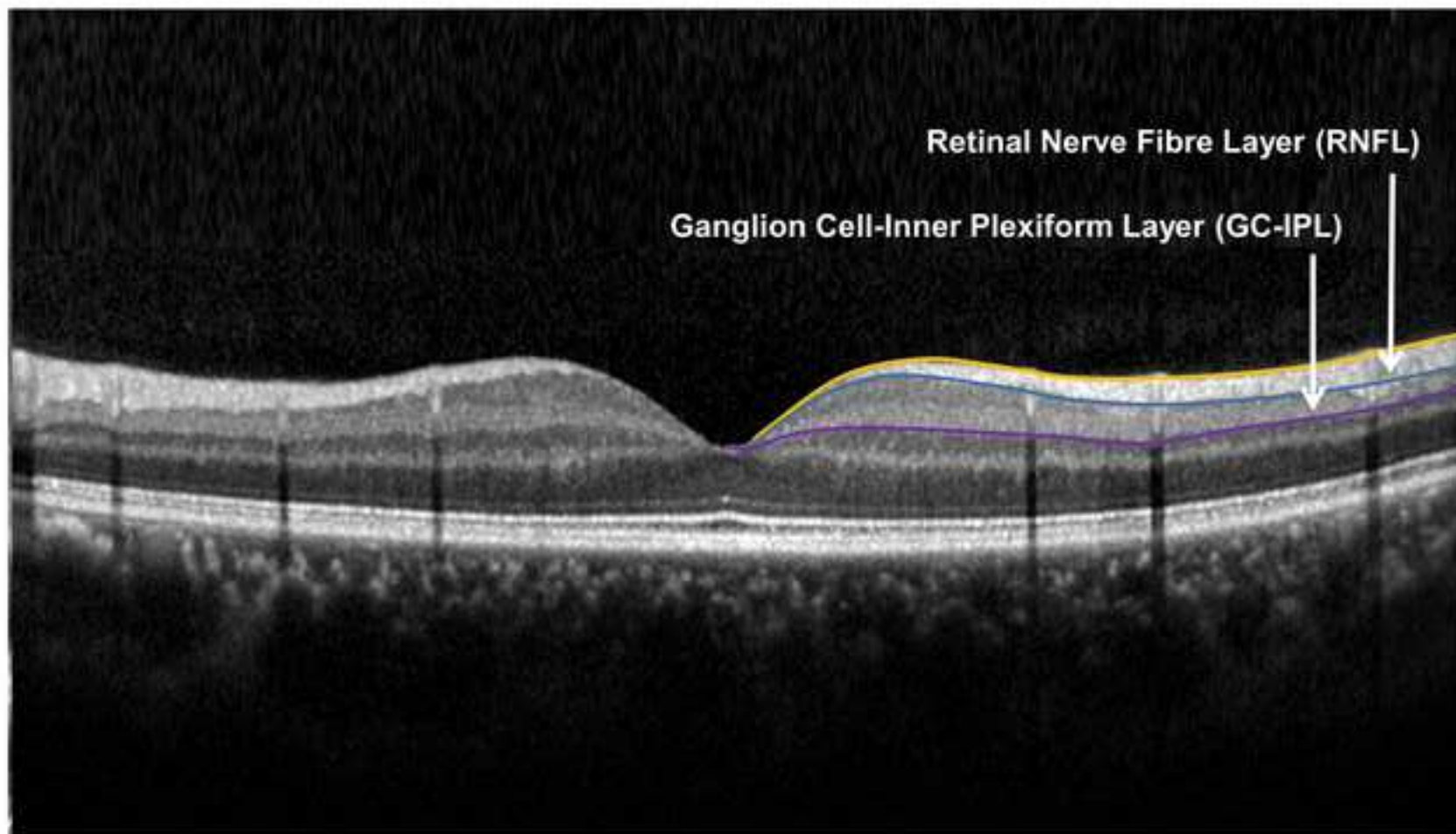


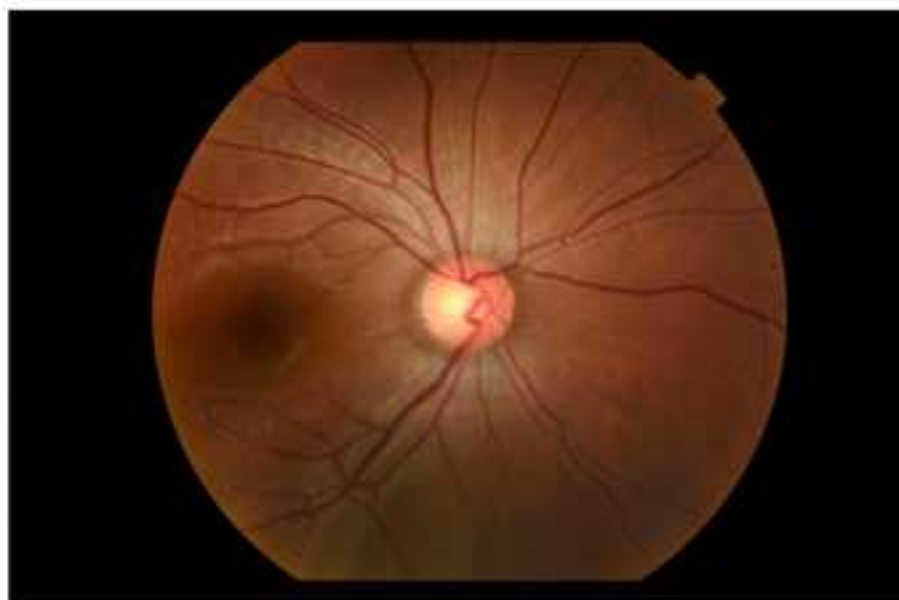


(A) Signal Strength < 6



(B) Motion Artifact



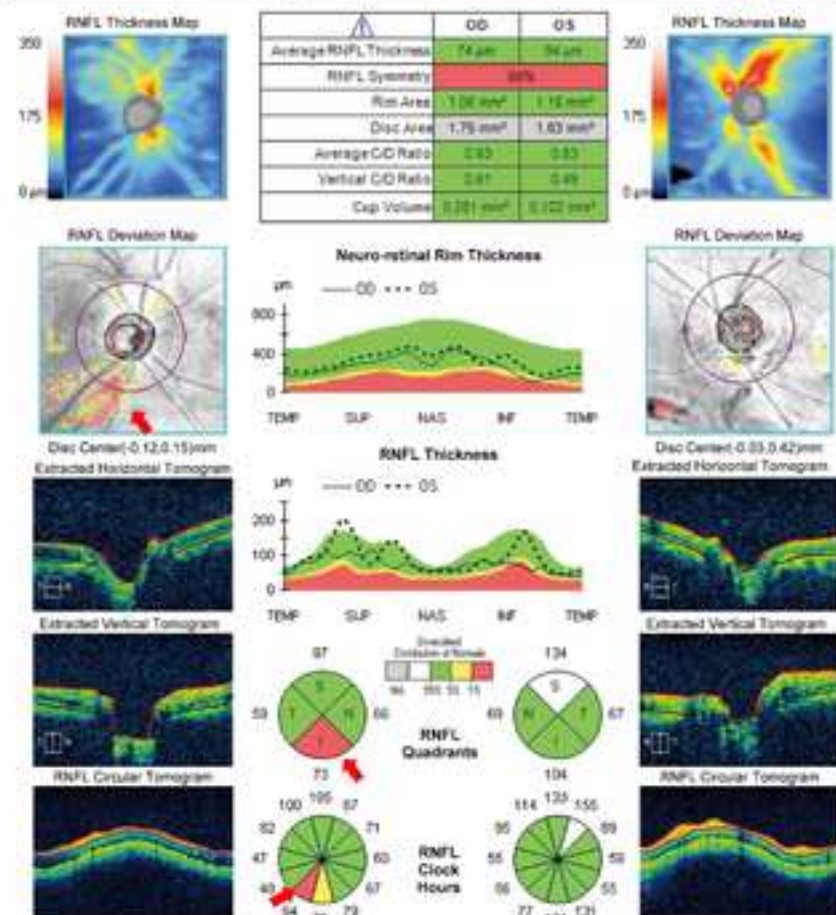


(A) Normal Subject



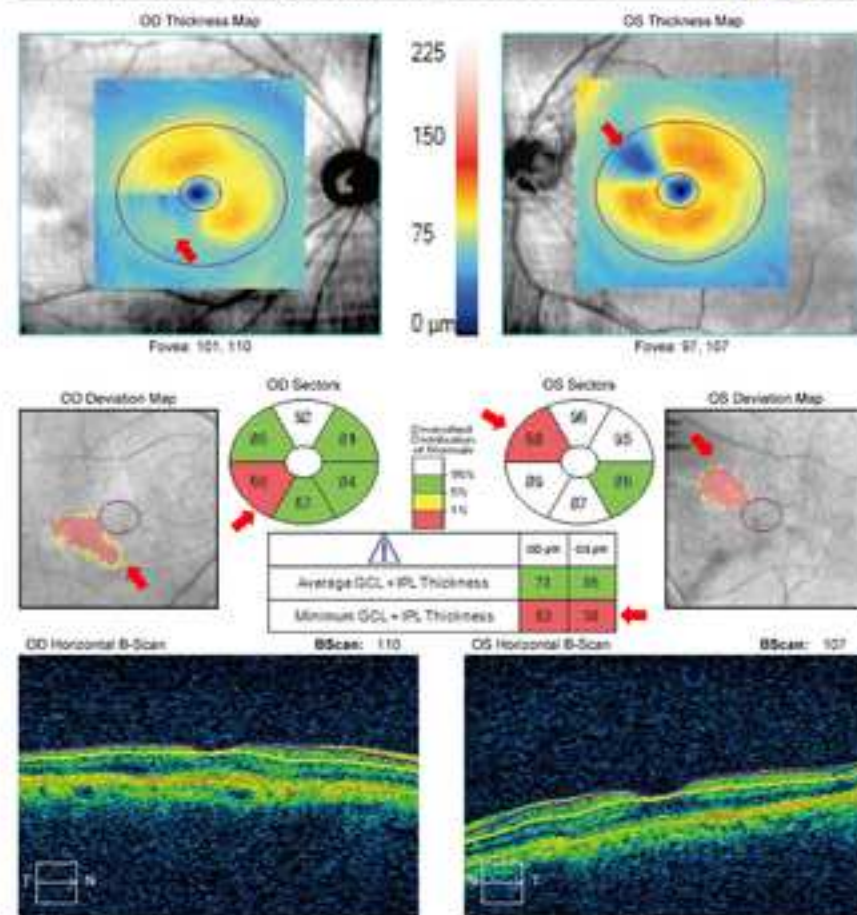
(B) AD Subject

ONH and RNFL OU Analysis: Optic Disc Cube 200x200 OD OS

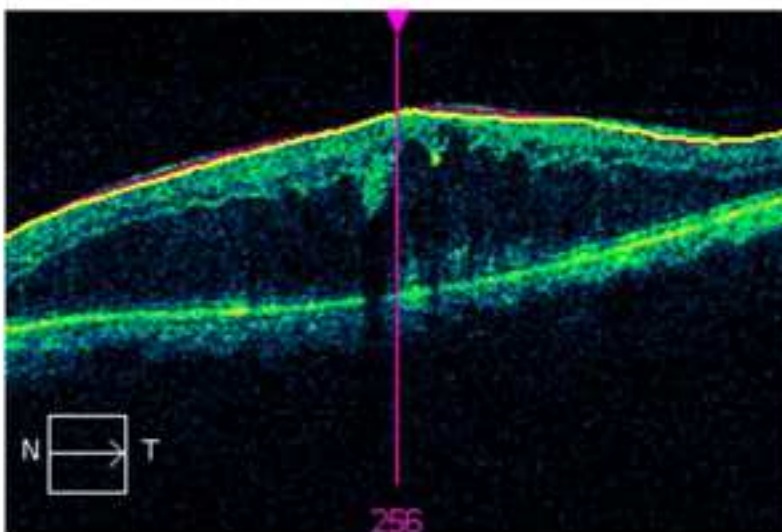


(A) Analysis Printout of the RNFL Thickness

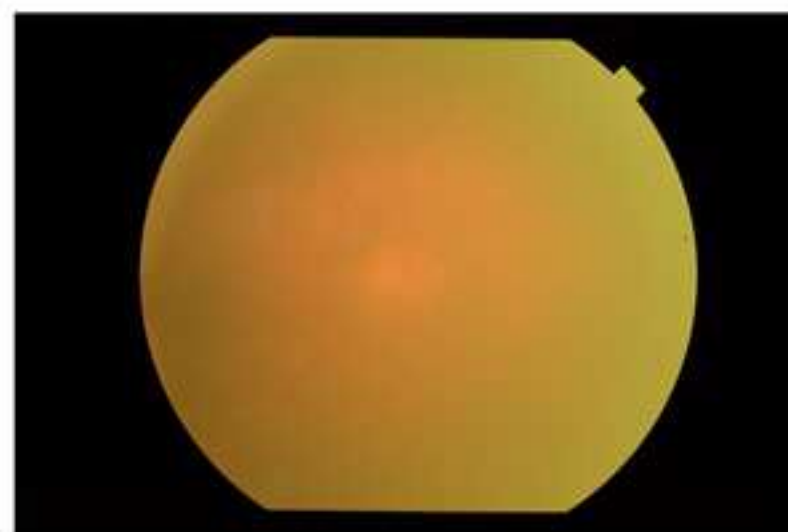
Ganglion Cell OU Analysis: Macular Cube 200x200 OD OS



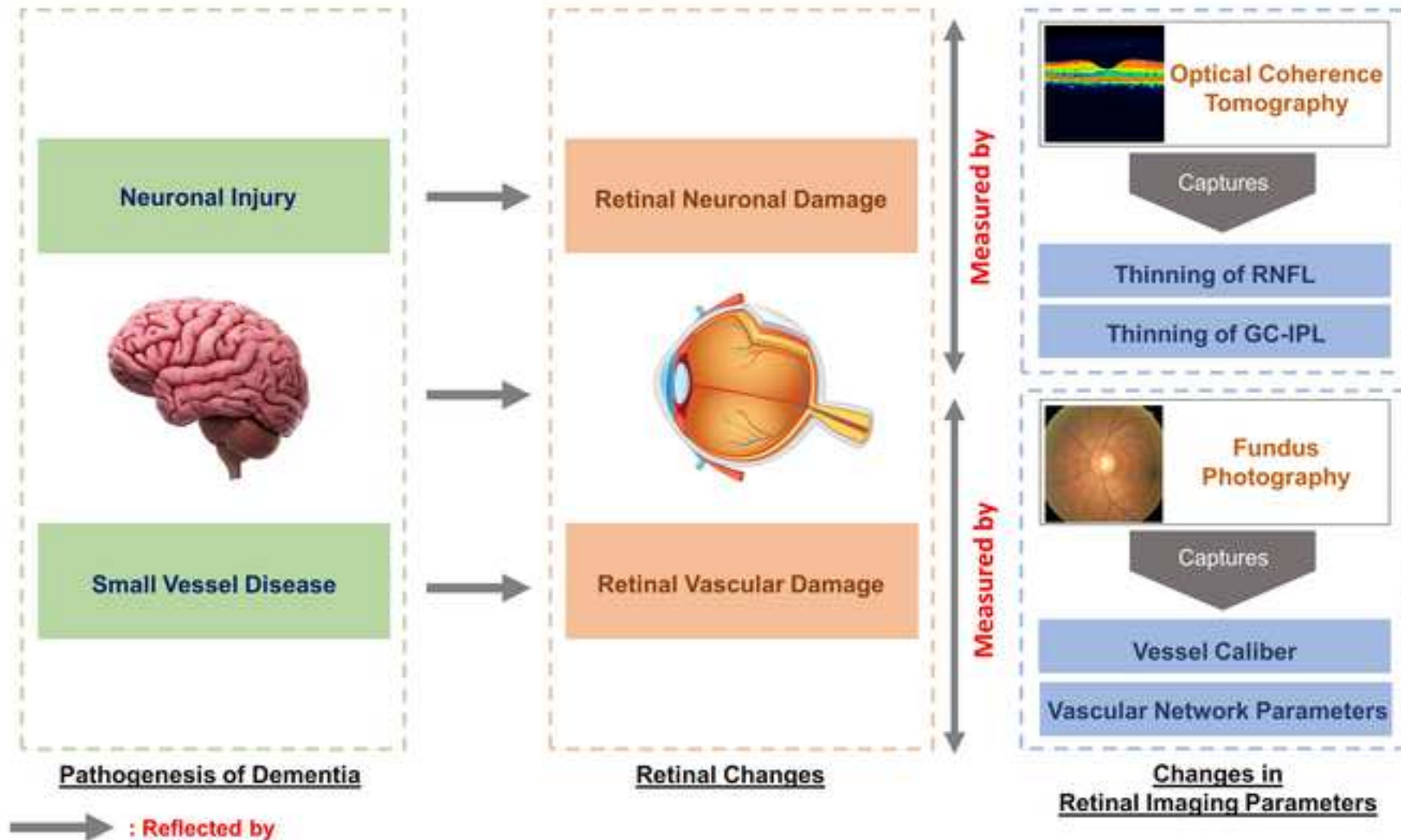
(B) Analysis Printout of the GC-IPL Thickness



**(A) Segmentation Failure
due to Diabetic Macular Edema**



(B) Media Opacity



	AD	Normal
CRAE of Zone B (μm)	116.4	156.4
CRVE of Zone B (μm)	186.9	207.5
CRAE of Zone C (μm)	138.5	165.8
CRVE of Zone C (μm)	206.6	232.2
Total Fractal Dimension	1.472	1.517
Arteriolar Fractal Dimension	1.246	1.316
Venular Fractal Dimension	1.253	1.273
Arteriolar Tortuosity (x10 ⁴)	0.61	0.48
Venular Tortuosity (x10 ⁴)	1.41	0.50
Arteriolar Branching Coefficient	2.43	1.49
Arteriolar Branching Angle (deg)	67.17	81.16
Venular Branching Coefficient	1.42	1.62
Venular Branching Angle (deg)	60.11	73.19

Parameter	Measured Zone	Interpretation and Reported Association with AD
Retinal Vessel Caliber		
Central Retinal Arteriolar Equivalent (CRAE)	Zone B & C	<ul style="list-style-type: none"> ➤ Changes in Central retinal arteriolar equivalent (CRAE) and central retinal venular equivalent (CRVE) indicate generalized retinal vessel narrowing or widening, and may suggest subtle microvascular dysfunction³⁵. ➤ It has been reported that increased CRVE is associated with incident dementia⁴⁶, vascular dementia⁴⁶, and decreased CRVE and CRAE is associated with Alzheimer's Disease^{47,48}.
Central Retinal Venular Equivalent (CRVE)	Zone B & C	
Retinal Vascular Network Parameters		
Fractal Dimensions (dF)	Zone C	<ul style="list-style-type: none"> ➤ Fractal dimension represents a “macro” measure that summarizes the branching complexity of the retinal vascular network³⁰; a larger value indicate a more complex branching pattern. ➤ It has been suggested that reduced retinal fractal dimension was associated with dementia^{47,48,59} and cognitive function⁶⁰.
Tortuosity (TORT)	Zone C	<ul style="list-style-type: none"> ➤ Reflects the general straightness of the retinal vessels, with a smaller tortuosity value indicates straighter retinal vessels ➤ It has been suggested that increased venular tortuosity and arteriolar tortuosity are associated with AD⁶²
Branching Angle (BA)	Zone C	<ul style="list-style-type: none"> ➤ The optimal value for the BA is approximately 75°³⁶ ➤ Alteration in branching angle may indicate changes in blood flow^{63,64}, endothelial dysfunction^{65,66} and attenuation in oxygen saturation⁶⁷.
Branching Coefficient (BC)	Zone C	<ul style="list-style-type: none"> ➤ The optimal value should be approximately 1.26³⁶. ➤ Deviation from optimal value of BC may increase energy cost, reducing the efficiency of circulation and metabolic transport³⁷.

Name of Material/ Equipment	Company	Catalog Number	Comments/Description
Non-mydriatic Retinal Camera	Topcon, Inc, Tokyo, Japan	TRC 50DX	N/A
Singapore I Vessel Assessment Program	National University of Singapore	Version 4.0	N/A
CIRRUS HD-OCT	Carl Zeiss Meditec, Inc, Dublin, CA	Model 4000	N/A
Mydriatic Agents	N/A	N/A	Prepared from 1% tropicamide and 2.5% phenylephrine hydrochloride



1 Alewife Center #200
Cambridge, MA 02140
tel. 617.945.9051
www.jove.com

ARTICLE AND VIDEO LICENSE AGREEMENT

Title of Article:

Using Retinal Imaging to Study Dementia

Author(s):

Victor T.T. Chan, Tiffany H.K. Tso, Fangyao Tang, Vincent Mok, Christopher Chen, Tien Y. Wong, Carol Y. Cheung

Item 1 (check one box): The Author elects to have the Materials be made available (as described at

<http://www.jove.com/author>) via: ☒ Standard Access ☐ Open Access

Item 2 (check one box):

- ☒ The Author is NOT a United States government employee.
- ☐ The Author is a United States government employee and the Materials were prepared in the course of his or her duties as a United States government employee.
- ☐ The Author is a United States government employee but the Materials were NOT prepared in the course of his or her duties as a United States government employee.

ARTICLE AND VIDEO LICENSE AGREEMENT

1. **Defined Terms.** As used in this Article and Video License Agreement, the following terms shall have the following meanings: “**Agreement**” means this Article and Video License Agreement; “**Article**” means the article specified on the last page of this Agreement, including any associated materials such as texts, figures, tables, artwork, abstracts, or summaries contained therein; “**Author**” means the author who is a signatory to this Agreement; “**Collective Work**” means a work, such as a periodical issue, anthology or encyclopedia, in which the Materials in their entirety in unmodified form, along with a number of other contributions, constituting separate and independent works in themselves, are assembled into a collective whole; “**CRC License**” means the Creative Commons Attribution-Non Commercial-No Derivs 3.0 Unported Agreement, the terms and conditions of which can be found at: <http://creativecommons.org/licenses/by-nc-nd/3.0/legalcode>; “**Derivative Work**” means a work based upon the Materials or upon the Materials and other pre-existing works, such as a translation, musical arrangement, dramatization, fictionalization, motion picture version, sound recording, art reproduction, abridgment, condensation, or any other form in which the Materials may be recast, transformed, or adapted; “**Institution**” means the institution, listed on the last page of this Agreement, by which the Author was employed at the time of the creation of the Materials; “**JoVE**” means MyJoVE Corporation, a Massachusetts corporation and the publisher of *The Journal of Visualized Experiments*; “**Materials**” means the Article and / or the Video; “**Parties**” means the Author and JoVE; “**Video**” means any video(s) made by the Author, alone or in conjunction with any other parties, or by JoVE or its affiliates or agents, individually or in collaboration with the Author or any other parties, incorporating all or any portion of the Article, and in which the Author may or may not appear.

2. **Background.** The Author, who is the author of the Article, in order to ensure the dissemination and protection of the Article, desires to have the JoVE publish the Article and create and transmit videos based on the Article. In furtherance of such goals, the Parties desire to memorialize in this Agreement the respective rights of each Party in and to the Article and the Video.

3. **Grant of Rights in Article.** In consideration of JoVE agreeing to publish the Article, the Author hereby grants to JoVE, subject to **Sections 4 and 7** below, the exclusive, royalty-free, perpetual (for the full term of copyright in the Article, including any extensions thereto) license (a) to publish, reproduce, distribute, display and store the Article in all forms, formats and media whether now known or hereafter developed (including without limitation in print, digital and electronic form) throughout the world, (b) to translate the Article into other languages, create adaptations, summaries or extracts of the Article or other Derivative Works (including, without limitation, the Video) or Collective Works based on all or any portion of the Article and exercise all of the rights set forth in (a) above in such translations, adaptations, summaries, extracts, Derivative Works or Collective Works and (c) to license others to do any or all of the above. The foregoing rights may be exercised in all media and formats, whether now known or hereafter devised, and include the right to make such modifications as are technically necessary to exercise the rights in other media and formats. If the “Open Access” box has been checked in **Item 1** above, JoVE and the Author hereby grant to the public all such rights in the Article as provided in, but subject to all limitations and requirements set forth in, the CRC License.

ARTICLE AND VIDEO LICENSE AGREEMENT

4. Retention of Rights in Article. Notwithstanding the exclusive license granted to JoVE in **Section 3** above, the Author shall, with respect to the Article, retain the non-exclusive right to use all or part of the Article for the non-commercial purpose of giving lectures, presentations or teaching classes, and to post a copy of the Article on the Institution's website or the Author's personal website, in each case provided that a link to the Article on the JoVE website is provided and notice of JoVE's copyright in the Article is included. All non-copyright intellectual property rights in and to the Article, such as patent rights, shall remain with the Author.

5. Grant of Rights in Video – Standard Access. This **Section 5** applies if the "Standard Access" box has been checked in **Item 1** above or if no box has been checked in **Item 1** above. In consideration of JoVE agreeing to produce, display or otherwise assist with the Video, the Author hereby acknowledges and agrees that, Subject to **Section 7** below, JoVE is and shall be the sole and exclusive owner of all rights of any nature, including, without limitation, all copyrights, in and to the Video. To the extent that, by law, the Author is deemed, now or at any time in the future, to have any rights of any nature in or to the Video, the Author hereby disclaims all such rights and transfers all such rights to JoVE.

6. Grant of Rights in Video – Open Access. This **Section 6** applies only if the "Open Access" box has been checked in **Item 1** above. In consideration of JoVE agreeing to produce, display or otherwise assist with the Video, the Author hereby grants to JoVE, subject to **Section 7** below, the exclusive, royalty-free, perpetual (for the full term of copyright in the Article, including any extensions thereto) license (a) to publish, reproduce, distribute, display and store the Video in all forms, formats and media whether now known or hereafter developed (including without limitation in print, digital and electronic form) throughout the world, (b) to translate the Video into other languages, create adaptations, summaries or extracts of the Video or other Derivative Works or Collective Works based on all or any portion of the Video and exercise all of the rights set forth in (a) above in such translations, adaptations, summaries, extracts, Derivative Works or Collective Works and (c) to license others to do any or all of the above. The foregoing rights may be exercised in all media and formats, whether now known or hereafter devised, and include the right to make such modifications as are technically necessary to exercise the rights in other media and formats. For any Video to which this Section 6 is applicable, JoVE and the Author hereby grant to the public all such rights in the Video as provided in, but subject to all limitations and requirements set forth in, the CRC License.

7. Government Employees. If the Author is a United States government employee and the Article was prepared in the course of his or her duties as a United States government employee, as indicated in **Item 2** above, and any of the licenses or grants granted by the Author hereunder exceed the scope of the 17 U.S.C. 403, then the rights granted hereunder shall be limited to the maximum rights permitted under such

statute. In such case, all provisions contained herein that are not in conflict with such statute shall remain in full force and effect, and all provisions contained herein that do so conflict shall be deemed to be amended so as to provide to JoVE the maximum rights permissible within such statute.

8. Likeness, Privacy, Personality. The Author hereby grants JoVE the right to use the Author's name, voice, likeness, picture, photograph, image, biography and performance in any way, commercial or otherwise, in connection with the Materials and the sale, promotion and distribution thereof. The Author hereby waives any and all rights he or she may have, relating to his or her appearance in the Video or otherwise relating to the Materials, under all applicable privacy, likeness, personality or similar laws.

9. Author Warranties. The Author represents and warrants that the Article is original, that it has not been published, that the copyright interest is owned by the Author (or, if more than one author is listed at the beginning of this Agreement, by such authors collectively) and has not been assigned, licensed, or otherwise transferred to any other party. The Author represents and warrants that the author(s) listed at the top of this Agreement are the only authors of the Materials. If more than one author is listed at the top of this Agreement and if any such author has not entered into a separate Article and Video License Agreement with JoVE relating to the Materials, the Author represents and warrants that the Author has been authorized by each of the other such authors to execute this Agreement on his or her behalf and to bind him or her with respect to the terms of this Agreement as if each of them had been a party hereto as an Author. The Author warrants that the use, reproduction, distribution, public or private performance or display, and/or modification of all or any portion of the Materials does not and will not violate, infringe and/or misappropriate the patent, trademark, intellectual property or other rights of any third party. The Author represents and warrants that it has and will continue to comply with all government, institutional and other regulations, including, without limitation all institutional, laboratory, hospital, ethical, human and animal treatment, privacy, and all other rules, regulations, laws, procedures or guidelines, applicable to the Materials, and that all research involving human and animal subjects has been approved by the Author's relevant institutional review board.

10. JoVE Discretion. If the Author requests the assistance of JoVE in producing the Video in the Author's facility, the Author shall ensure that the presence of JoVE employees, agents or independent contractors is in accordance with the relevant regulations of the Author's institution. If more than one author is listed at the beginning of this Agreement, JoVE may, in its sole discretion, elect not take any action with respect to the Article until such time as it has received complete, executed Article and Video License Agreements from each such author. JoVE reserves the right, in its absolute and sole discretion and without giving any reason therefore, to accept or decline any work submitted to JoVE. JoVE and its employees, agents and independent contractors shall have

ARTICLE AND VIDEO LICENSE AGREEMENT

full, unfettered access to the facilities of the Author or of the Author's institution as necessary to make the Video, whether actually published or not. JoVE has sole discretion as to the method of making and publishing the Materials, including, without limitation, to all decisions regarding editing, lighting, filming, timing of publication, if any, length, quality, content and the like.

11. **Indemnification.** The Author agrees to indemnify JoVE and/or its successors and assigns from and against any and all claims, costs, and expenses, including attorney's fees, arising out of any breach of any warranty or other representations contained herein. The Author further agrees to indemnify and hold harmless JoVE from and against any and all claims, costs, and expenses, including attorney's fees, resulting from the breach by the Author of any representation or warranty contained herein or from allegations or instances of violation of intellectual property rights, damage to the Author's or the Author's institution's facilities, fraud, libel, defamation, research, equipment, experiments, property damage, personal injury, violations of institutional, laboratory, hospital, ethical, human and animal treatment, privacy or other rules, regulations, laws, procedures or guidelines, liabilities and other losses or damages related in any way to the submission of work to JoVE, making of videos by JoVE, or publication in JoVE or elsewhere by JoVE. The Author shall be responsible for, and shall hold JoVE harmless from, damages caused by lack of sterilization, lack of cleanliness or by contamination due to the making of a video by JoVE its employees, agents or independent contractors. All sterilization, cleanliness or decontamination procedures shall be solely the responsibility of the Author and shall be undertaken at the Author's

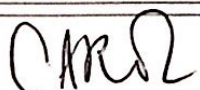
expense. All indemnifications provided herein shall include JoVE's attorney's fees and costs related to said losses or damages. Such indemnification and holding harmless shall include such losses or damages incurred by, or in connection with, acts or omissions of JoVE, its employees, agents or independent contractors.

12. **Fees.** To cover the cost incurred for publication, JoVE must receive payment before production and publication the Materials. Payment is due in 21 days of invoice. Should the Materials not be published due to an editorial or production decision, these funds will be returned to the Author. Withdrawal by the Author of any submitted Materials after final peer review approval will result in a US\$1,200 fee to cover pre-production expenses incurred by JoVE. If payment is not received by the completion of filming, production and publication of the Materials will be suspended until payment is received.

13. **Transfer, Governing Law.** This Agreement may be assigned by JoVE and shall inure to the benefits of any of JoVE's successors and assignees. This Agreement shall be governed and construed by the internal laws of the Commonwealth of Massachusetts without giving effect to any conflict of law provision thereunder. This Agreement may be executed in counterparts, each of which shall be deemed an original, but all of which together shall be deemed to be one and the same agreement. A signed copy of this Agreement delivered by facsimile, e-mail or other means of electronic transmission shall be deemed to have the same legal effect as delivery of an original signed copy of this Agreement.

A signed copy of this document must be sent with all new submissions. Only one Agreement required per submission.

CORRESPONDING AUTHOR:

Name:	Carol Y. Cheung	
Department:	Department of Ophthalmology and Visual Sciences	
Institution:	The Chinese University of Hong Kong	
Article Title:	Using Retinal Imaging to Study Dementia	
Signature:		Date: 18 April 2017

Please submit a signed and dated copy of this license by one of the following three methods:

- 1) Upload a scanned copy of the document as a pdf on the JoVE submission site;
- 2) Fax the document to +1.866.381.2236;
- 3) Mail the document to JoVE / Attn: JoVE Editorial / 1 Alewife Center #200 / Cambridge, MA 02139

For questions, please email submissions@jove.com or call +1.617.945.9051

Department of Ophthalmology and Visual Sciences 眼科及視覺科學學系**The Chinese University of Hong Kong 香港中文大學**

Hong Kong Eye Hospital, 147K Argyle Street, Kowloon, Hong Kong 香港九龍亞皆老街147K號香港眼科醫院
tel: (852) 3943 5855 • fax: (852) 2715 9490 • <http://www.ovs.cuhk.edu.hk> • e-mail: deptovs@cuhk.edu.hk

Prince of Wales Hospital Eye Centre 威爾斯親王醫院眼科中心

Shatin, N.T., Hong Kong 香港新界沙田 • tel: (852) 2632 2879 • fax: (852) 2648 2943

Joint Santou International Eye Center of Shantou University and The Chinese University of Hong Kong (JSIEC) 汕頭大學 • 香港中文大學聯合汕頭國際眼科中心

Dong Xia North Road, Shantou 515041, Guangdong Province, China 中國廣東省汕頭市東廈北路

tel: (86) 754 8839 3527 • fax: (86) 754 8839 3501 • <http://www.jsiec.org> • e-mail: admin@jsiec.org



30th May, 2017

Dr. Mala Mani

Review Editor

Journal of Visualized Experiments

Dear Dr. Mani,

Manuscript#: JoVE56137
Using Retinal Imaging to Study Dementia

Thank you very much for the review of the above manuscript. We are pleased to address the comments raised in the review and have included the Reviewers' suggestions in the enclosed revised manuscript. The changes/additions in the revised manuscript are identified in the track changes. The current word count is 7,427 for the text of the manuscript and 143 for the long abstract.

Editorial Comments:

1) The Protocol should contain only action items that direct the reader to do something. Please move the discussion about the procedure to the Results or Discussion section. "Notes" should be concise and used sparingly. They should only be used to provide extraneous details/optional steps/recommendations that are not critical to a step. Please move Sections 2, 3 and 4 NOTES to the results or discussion sections.

Authors' response:

Thank you. Most "Notes" have now been moved to the results or discussion sections, unless necessary:

- (1) Two Notes that indicate the pause steps of the protocol
- (2) A note stating that the SIVA program can be substituted by other computer-assisted analysis programs:

- 2.2. Open the images in the computer-assisted analysis program for automatic tracing.

Note: The SIVA program is used for illustration purpose only and can be substituted by other available measurement programs.

- (3) A note that describe the morphological differences between arterioles and venules, which provides details and guidance to step 2.3.2:

- 2.3.2 Left click to select the vessels with incorrect vessel label (arterioles vs venules) and click the "Vessel (T)ype" button to change the vessel type.

Note: Arterioles can be distinguished from venules based on their physiological differences. For e.g. venules are in general darker in color and wider than arterioles. Vessels with same vessel type do not cross each other. Arterioles are labelled in red and venules are labelled in blue.



(4) A note that explain the meaning of “vessel covers”:

- 2.4.1 Click the “Find Covers” button to lay vessel covers on all vessel segments automatically.

Note: Vessel covers are measurement lines that estimate the approximate width of the internal lumens of the vessels.

(5) A note stating that which steps can be automatically done by the computer-assisted analysis program:

- Note: Steps 3.1 to 3.7 can be completed automatically by a computer-assisted analysis program
- Note: Steps 4.2.2.1 to 4.2.2.4 can be automatically completed by the analysis algorithm.
- Note: Steps 4.3.2.1 to 4.3.2.6 can be automatically completed by the analysis algorithm.

(6) A note that explains the size and shape of the elliptical annulus, which is used to assess the GC-IPL thickness.

- Note: The size and shape of the elliptical annulus conform closely to the macular anatomy and thus correspond to the area where the RGCs are thickest in normal eyes^{33,34}. The area within the inner ring of the annulus is not measured as the macular GC-IPL in this area is very thin and difficult to detect accurately.

2) Section 3: Please re-write this in the imperative tense and provide stepwise detail on how to perform the retinal vasculature measurement.

Authors' response: Thank you. This section has now been re-written in the imperative tense to illustrate the procedures of measuring retinal vasculature. We would like to highlight that the steps described in this section can be completed automatically by the computer-assisted program. Hence, we decided to place more emphasis on the steps of manually adjusting the vessel tracings, instead of providing too much details on this section. The revisions are quoted as follows:

- 3. Measure the retinal vascular parameters using a computer-assisted program.

Note: Steps 3.1 to 3.7 can be completed automatically by a computer-assisted analysis program

3.1 Open the fundus photograph to be measured.

3.2 Place four concentric circles as measurement grids using the centre of optic disc as a reference (Figure 6A). Label the area 0.5-1.0 disc diameters away from the disc margin as zone B, and the area 0.5-2.0 disc diameters away from the disc margin as zone C¹⁸ (Figure 6A), according to the modified protocol of Atherosclerosis Risk in Communities (ARIC) study¹⁹.

3.3 Measure retinal vascular caliber from both zone B and zone C, using a method modified from the ARIC study¹⁹ (Figure 6B), which has been widely adopted in many large population studies²⁰⁻²⁶.

3.3.1 Measure the lengths of vessel covers in the six largest arterioles and the six largest venules to estimate retinal vessel calibers.

3.3.2 Summarize the retinal arteriolar and venular calibers as central retinal artery equivalent (CRAE) and central retinal vein equivalent (CRVE) respectively¹⁷, using the revised Knudtson–Parr–Hubbard formula^{18,19}.

[Place New Figure 6 Here]

3.4 Identify all vessels in zone C with a width $>40\ \mu\text{m}$. Calculate the retinal arteriolar and venular tortuosity from the integral of the total squared curvature along the vessel paths and normalize the value with the total arc length, bowing, and points of inflection^{27,28}.

3.5 Compute the total, arteriolar, and venular fractal dimensions from zone C, using an established method called “box-counting method”²⁹⁻³¹.

3.5.1 Divide the retinal image into a series of equally sized square boxes.

3.5.2 Count the number of boxes containing a section of the skeletonized line tracing.

3.5.3 Repeat the process with a series of different sized boxes.

3.5.4 Plot the logarithm of the number of boxes containing the line tracing against the logarithm of the size of the boxes, and calculate the slope of the line, which is the fractal dimension.

3.6 Identify vessels with first bifurcation in zone C and calculate the angles (θ) subtended between first two daughter vessels³² (Figure 6C). Compute the mean value to obtain the average branching angle.

3.7 Calculate the branching coefficient from zone C using the formula:
 $(d_1^2 + d_2^2)/d_0^2$, where d_0 is the mean trunk caliber, d_1 and d_2 are the mean branch calibers (Figure 6C).

3) Section 4: Please adjust the numbering in this section.

Authors' response: Thank you. The numbering of all sections (including section 4) has now been adjusted.

4) 4.1.1.6: Using which similar methods? Please specify the step numbers.

Authors' response: Steps 4.1.1.6 has now been re-numbered into 4.1.6 and revised as follows:

- 4.1.6 Perform an optic nerve head scan with the “Optic Disc Cube” scanning protocol using steps 4.1.2 to 4.1.5 (Figure 7B).

5) 4.1.1.8: Save images as what file type?

Authors' response: Thank you. The images captured by the OCT are normally saved as built-in-program-specific file format and stored within the program. In other words, researchers are not required to choose the file type after the image acquisition process. For this reason, the file type is not specified in the protocol. To avoid confusion, 4.1.1.8 has now been revised as:

- 4.1.8 Save the scanning results.

For your information, steps 4.1.1.8 has now been re-numbered into 4.1.8.

6) 4.1.3: Please re-write this in the imperative tense and provide stepwise detail on how to perform the measurement.

Authors' response:

Thank you. This step has now been revised and renumbered, as follows:

- 4.2. Generate the analysis printout of the macular GC-IPL thickness.

4.2.1 Select the “Macular Cube” scan records of both eyes in the analysis interface

4.2.2 Click the “Ganglion Cell OU Analysis” to initiate the automatic analysis algorithm to assess the GC-IPL thickness of the captured image (Figure 7E).

Note: Steps 4.2.2.1 to 4.2.2.4 can be automatically completed by the analysis algorithm.

4.2.2.1 Generate a 14.13 mm² fovea-centered elliptical annulus, which has horizontal inner and outer radius of 0.6mm and 2.4 mm respectively, and vertical inner and outer radius of 0.5 mm and 2.0 mm respectively.

Note: The size and shape of the elliptical annulus conform closely to the macular anatomy and thus correspond to the area where the RGCs are thickest in normal eyes^{33,34}. The area within the inner ring of the annulus is not measured as the macular GC-IPL in this area is very thin and difficult to detect accurately.

4.2.2.2 Segment the outer boundary of the RNFL and the outer boundary of the inner plexiform layer (IPL) to locate the GC-IPL (Figure 9).

4.2.2.3 Measure the (a) average, (b) minimum and (c) six sectorial (superotemporal, superior, superonasal, inferonasal, inferior, inferotemporal) thickness of macular GC-IPL within the fovea-centered elliptical annulus.

4.2.2.4 Report the measurement results on an analysis printout

4.2.3 Save the analysis printout as pdf format.



[Place New Figure 9 Here]

4.3. Generate the analysis printout of the RNFL thickness (Figure 7F)

4.3.1 Select the “Optic Disc Cube” scan records of both eyes in the analysis interface

4.3.2 Click the “ONH and RNFL OU Analysis” to initiate the automatic analysis algorithm to assess the RNFL thickness of the captured image.

Note: Steps 4.3.2.1 to 4.3.2.6 can be automatically completed by the analysis algorithm.

4.3.2.1 Measure the RNFL thickness at each scan point and generate an RNFL thickness map.

4.3.2.2 Identify the optic disc by detecting a dark spot near the center of the scan that has a size and shape consistent with a range of optic disc.

4.3.2.2 Position a calculation circle of 3.46 mm in diameter around the optic disc on the RNFL thickness map.

4.3.2.3 Measure and calculate the (a) global, (b) four-quadrants (temporal, superior, nasal and inferior), and (c) twelve-clock-hour parapapillary RNFL thickness, using the calculation circle as regions of interest (ROI).

4.3.2.4 Compare the measured RNFL thickness to the device’s internal normative age-matched database and generate a deviation map and a significance map.

4.3.2.5 Report the measurement results on an analysis printout

4.3.3 Save the analysis printout as pdf format.

7) Please highlight 2.75 pages or less of text (which includes headings and spaces) to identify which steps should be visualized to tell the most cohesive story of your protocol steps. Please see JoVE’s instructions for authors for more clarification. Remember that the non-highlighted protocol steps will remain in the manuscript and therefore will still be available to the reader.

Authors’ response: Thank you. Less than 2.75 pages of steps have been highlighted to identify the steps for visualization.

8) Results: Please confine to the results obtained by the authors in this section. Please move the discussion about other works to the Discussion section.

Authors’ response: Thank you. The results and the discussion section have now been revised accordingly.



9) Please provide scale bars for microscope images if possible.

Authors' response: Thank you. The size of the OCT images and the fundus photographs has been defined in the associated legends, as follows:

- “Figure 2: Optimal and suboptimal fundus photographs. The image quality of fundus photographs directly affects the measurement and analysis of the retinal microvasculature. Hence, quality of fundus photographs must be checked immediately after image acquisition. The image should be discarded if one of these artefacts is observed. **These images were captured using 50-degree fundus camera.**”

Figure 10: An example to show the differences in retinal vasculature between a normal subject and an AD subject.

.....

These images were captured using 50-degree fundus camera and were analyzed using the method described in the protocol.

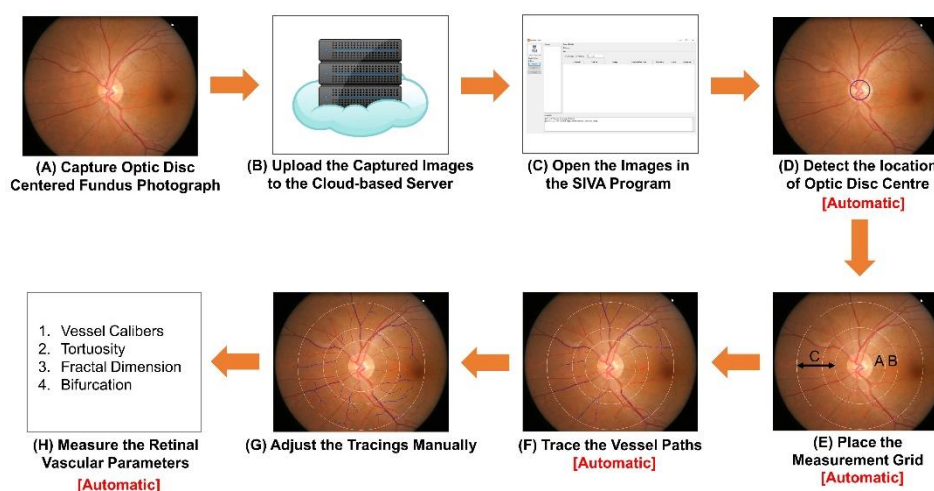
- Figure 11: Analysis printout of the retinal neuronal structure from a subject with AD.

.....

The scanning area of the images in the analysis printout is 6 mm x 6 mm.

10) Figure 1: Please replace panel b without the branding “Retina”.

Author's response: Thank you. The figure has now been redrawn as follows:



11) Figure 7: Please provide a general description of each panel and refer to the panels in the legend.

Authors' response: Thank you. The legend has now been revised as follows:

- Figure 7: Image acquisition and optimal results of retinal neuronal structure analysis. Optical coherence tomography (OCT) is used to measure the thickness of the ganglion cell-inner plexiform layer (GC-IPL) and retinal nerve fibre layer (RNFL). (A, B): The GC-IPL and RNFL can be imaged using the built-in “macular cube” and “optic disc cube” scanning protocols respectively. (C, D): It is critical to check the image quality immediately after image acquisition. Discard the image and retake the scan if the signal strength is smaller than 6, or motion artifacts are detected. (E, F): After finishing the image acquisition, the built-in algorithm can automatically analyze the image and generate a report for interpretation.

12) Figure 10: Please provide the values of measurements in the form of a .xls Table. For e.g. the values of average lengths of the vessel, vessel caliber, network parameters, bifurcation geometry, etc. of both normal and AD subjects obtained using your method.

Authors' response: Thank you. The retinal vascular parameters of both normal and AD subjects in Figure 10 have been included in “New Table 1 (20170530)”.

13) Figure 10 Lines 605-609 (these finding are...further evaluation): Please move these lines to the results section.

Authors' response: The legend has now been revised as follows:

- Figure 10: An example to show the differences in retinal vasculature between a normal subject and an AD subject. (A) Fundus photographs of a healthy subject showing wider vessel caliber (CRAE of Zone B, 156.45 μm ; CRVE of Zone B, 207.54 μm ; CRAE of Zone C, 165.82 μm ; CRVE of Zone C, 232.22 μm), higher retinal vascular fractal dimension (total fractal dimension, 1.517; arteriolar fractal dimension, 1.316; venular fractal dimension, 1.273) and smaller retinal vascular tortuosity (arteriolar tortuosity [104], 0.476; venular tortuosity [104], 0.501). (B) Fundus photographs of an AD subject showing narrower vessel caliber (CRAE of Zone B, 116.38 μm ; CRVE of Zone B, 186.93 μm ; CRAE of Zone C, 138.47 μm ; CRVE of Zone C, 206.61 μm), smaller retinal vascular fractal dimension (total fractal dimension, 1.472; arteriolar fractal dimension, 1.246; venular fractal dimension, 1.253) and higher retinal vascular tortuosity (arteriolar tortuosity [104], 0.613; venular tortuosity [104], 1.41). These images were captured using 50-degree fundus camera and were analyzed using the method described in the protocol.

14) Figure 11: Please refer to panels A and B in the legend.

Authors' response: Thank you. The legend of Figure 11 has now been revised as follows:

- Figure 11: Analysis printout of the retinal neuronal structure from a subject with AD. The analysis printouts of both GC-IPL and RNFL thickness include three types of thickness



map, namely the thickness map, the deviation map and the significance map. (A) The red and yellow super-pixels in the right deviation map (red arrows) indicate the RNFL thickness of these parts of retina fell outside the 99% or within 95%–99% percentile range, respectively. Consistently, the decreased RNFL thickness of these regions is also indicated by the red and yellow sectors in the two significance maps, namely “RNFL quadrants” and “RNFL clock hours”. While the red sectors indicate the RNFL thickness fell outside the normal range ($p < 1\%$), the yellow sector indicates borderline values ($1\% < p < 5\%$). All together, these maps suggest that the RNFL thickness was reduced in the AD subject. (B) The interpretation of the GC-IPL thickness is similar to that of the RNFL thickness. In the AD subject, the thickness map shows more light blue areas (red arrows), which visualize the thinning of the GC-IPL. In line with this finding, the red and yellow super-pixels in the deviation maps (red arrows) also indicate the thickness of these regions fell outside the 99% or within 95%–99% percentile range, respectively. Reduction of GC-IPL thickness in these regions is also illustrated by the red sectors in the significance map.

15) Please complete the acknowledgement sentence.

Authors' response: Thank you. The acknowledgement sentence is now completed, as follows:

- We would like to express our appreciation to School of Computing, National University of Singapore for technical supports.

Please do not hesitate to contact us in case of any concerns. We look forward to a positive decision from *Journal of Visualized Experiments*.

Best regards,

Dr Carol Y. Cheung, on behalf of all co-authors.

Assistant Professor

Department of Ophthalmology and Visual Sciences

The Chinese University of Hong Kong

Hong Kong Eye Hospital

147K Argyle Street, Kowloon, Hong Kong

T: +852 39435831 / F: +852 27159490 / Email: carolcheung@cuhk.edu.hk

